A VARIABLE RESOLUTION STRETCHED GRID GENERAL CIRCULATION MODEL: REGIONAL CLIMATE SIMULATION

Michael S. Fox-Rabinovitz
Department of Meteorology/ESSIC, University of Maryland, College Park, MD 20742 and
Data Assimilation Office, Goddard Space Flight Center, Greenbelt, MD 20771

Lawrence L. Takacs and Ravi C. Govindaraju
General Sciences Corporation, 4600 Powder Mill Road, Beltsville, MD 20705-2675 and
Data Assimilation Office, Goddard Space Flight Center, Greenbelt, MD 20771

Max J. Suarez
Laboratory for Atmospheres, Goddard Space Flight Center, Greenbelt, MD 20771

Revised version submitted for publication to Monthly Weather Review

(March 2000)

Corresponding author address: Dr. Michael S. Fox-Rabinovitz,
ESSIC, CSS Bldg., University of Maryland, College Park, MD 20742
E-mail: foxrab@atmos.umd.edu

ABSTRACT

The development of and results obtained with a variable resolution stretched-grid GCM for the regional climate simulation mode,are presented. A global variable resolution stretched-grid used in the study has enhanced horizontal resolution over the U.S. as the area of interest.

The stretched-grid approach is an ideal tool for representing regional to global scale interactions. It is an alternative to the widely used nested grid approach introduced over a decade ago as a pioneering step in regional climate modeling.

The major results of the study are presented for the successful stretched-grid GCM simulation of the anomalous climate event of the 1988 U.S. summer drought. The straightforward (with no updates) two month simulation is performed with 60 km regional resolution. The major drought fields, patterns and characteristics such as the time averaged 500 hPa heights, precipitation, and the low level jet over the drought area, appear to be close to the verifying analyses for the stretched-grid simulation. In other words, the stretched-grid GCM provides an efficient down-scaling over the area of interest with enhanced horizontal resolution. It is also shown that the stretched-grid GCM skill is sustained throughout the simulation extended to one year.

The developed and tested in a simulation mode stretched-grid GCM is a viable tool for regional and subregional climate studies and applications.

1. Introduction

The widely-used nested-grid approach represents a pioneering first step towards reliable regional climate simulations (e.g. Dickinson et al. 1989, Pielke et al. 1992, Giorgi 1990,1995, Juang and Kanamitsu 1994, Caya and Laprise 1999, Pan et al. 1999).

The nested-grid approach to regional climate modeling was coming mostly from and was readily accepted and adopted by the regional forecast or LAM (limited area model) modelers as a natural extension and new application of this kind of models. The variable-resolution stretched-grid (SG) approach is coming mostly from the global or GCM modelers as a new application of global models in the variable resolution framework, with enhanced resolution for both prognostic fields and boundary forcing over the area of interest.

The variable-resolution stretched-grid forecast models have been first developed in the late 70's. They are successfully used for operational short-term, 24–48 hour, forecasting. At the CMC (Canadian Meteorological Center), a grid point model is used since the early 90's (Staniforth and Mitchell 1978, Staniforth and Daley 1979, Staniforth 1995, 1997, Cote et al. 1993, Cote 1997). Independently, in the late 80's the development of the variable resolution stretched-grid spectral model was started at Meteo-France (Courtier and Geleyn 1988) using the approach developed by Schmidt (1977). The model is used for operational short-term forecasting since the mid-90's (e.g. Yessad and Benard 1996). The first regional climate simulation was performed with the Meteo-France model in the mid-90's (Deque and Piedelievre 1995).

Other variable resolution models have been developed for regional applications (e.g. Paegle 1989, Hardiker 1997, McGregor and Katzfey 1998). The Goddard Earth Observing System (GEOS) stretched-grid (SG)-GCM is being developed by the authors since the mid-90's. At the first stage of the development, the SG-dynamical core in the Held-Suarez framework (Held and Suarez 1994) without orography (a flat surface) was developed and thoroughly tested in the simulation and medium-range integration modes (Fox-Rabinovitz et al. 1997). The dynamical core has the finite-difference dynamics identical to that of the GEOS GCM (Suarez and Takacs

1995,Takacs and Suarez 1996) and a Newtonian-type physics (Held and Suarez 1994). The finite-difference dynamics has been adjusted to a variable-resolution stretched-grid and the computational problems related to variable resolution have been successfully resolved. In the follow-up study with the dynamical core, a real orographic forcing was introduced. For the case, the filtering technique was refined, and the down-scaling effects were confirmed. The experiments with the SG-dynamical core have shown that the stretched-grid approach provides the efficient down-scaling over the area of interest. It appears to be a viable candidate for cost-effective regional modeling not only for a short-term but also for medium-range and, most importantly, for long-term regional integrations. It was an important step towards developing a full diabatic stretched-grid GCM.

Relying upon the obtained results, the authors concluded that the global stretched-grid approach has to be explored as an alternative methodology to the current widely used nested grid approach. The following comments outline some differences of the stretched vs. nested grid approach. The nested grid approach has the following advantages. The computational efficiency is high due to using a regional integration domain. There is the possibility of combining the outer hydrostatic GCM or reanalyses and an inner non-hydrostatic model. It is preferable to use the GCM physics for the inner model (e.g. Caya and Laprise 1999). There also exists the possibility of using a perturbation regional model (like the NCEP Regional Spectral Model (Juang and Kanamitsu 1994).

Due to the global integration domain for variable-resolution stretched-grid models there are no boundary conditions and no computational buffer around the area of interest is needed to control the boundary conditions problems. The global variable-resolution approach to regional climate modeling allows continuous/straightforward long-term integrations to be autonomously performed without the need for a driving GCM to provide a continuous or periodic updating of conditions at the region's boundaries, and, for early nested regional climate models, periodic re-initialization of conditions throughout the region of interest. It also avoids the need to apply

damping techniques within a computational buffer region. Both the updating and noise damping are required in nested-grid models to control severe computational noise arising from the application of lateral boundary conditions. A further advantage of variable-resolution stretched-grid models is that they provide self-consistent interactions between global and regional scales of motion and their associated phenomena. In other words, using one variable-resolution global model results in a better preservation of a delicate balance between global and regional scales. Also, there exists the possibility of introducing a mesoscale non-hydrostatic SG-GCM. The global non-hydrostatic models are being developed (e.g. Semazzi et al. 1995, Qian et al. 1998, Yeh et al. 1999), and the stretched-grid approach is a practical way to use them for regional integrations.

The stretched-grid approach provides the possibility to use such a fine regional resolution that is not available otherwise for GCMs. Actually, any GCM resolution can be made at least 2-4 times finer for the area of interest through the SG-approach. Depending on the regional resolution used, the computational savings are at least one order of magnitude compared to computer time needed for the corresponding control run with a global uniform fine grid GCM. Therefore, the variable-resolution stretched-grid models provide a scientifically and practically attractive possibility of performing cost-effective regional/subregional integrations with finer resolution over an area of interest than are likely to be possible in the foreseeable future with fine uniform global grid models (Cote 1997, Fox-Rabinovitz et al. 1997).

It is noteworthy that the computational efficiency provided by the stretched-grid approach, is not the only reason or rational for its practical implementation. It is at least equally or even more important that through this approach an efficient down-scaling is obtained representing fine and very fine regional mesoscale fields, diagnostics, and phenomena.

All the above considerations explain why the variable resolution stretched grid approach could be considered as a viable alternative candidate for regional climate modeling. At the same time we would like to emphasize that an optimal choice between using a nested or stretched-grid

approach should be carefully made for different applications. Also, the combination of two approaches may appear to be an attractive optimal choice.

Note that according to Lindzen and Fox-Rabinovitz (1989), the consistency of horizontal and vertical resolution should be preserved. Therefore, an increase of horizontal resolution has to be accompanied by the corresponding increase of vertical resolution. In this study we rely upon rather fine vertical resolution (70 layers) used for the SG-GCM experiments.

It is worth clarifying that the term "down-scaling" for a dynamical model or dynamical down-scaling is widely used for nested-grid models driven by a coarser resolution GCM or reanalyses. For the nested-grid models, this term is associated with the abrupt resolution change between the inner model and outer model or reanalysis forcing. It seems appropriate to adopt this term for the SG-approach that uses a stretched grid with gradually varying global resolution. As a result the large and medium synoptic scales are produced away from the region of interest while finer mesoscales are gradually introduced when approaching the area of interest (and its immediate vicinity). The efficiency of such a dynamical down-scaling for the SG-GCM regional simulation mode is investigated in the study.

The anomalous regional climate event of the U.S. 1988 summer drought drew a significant attention of climatologists and was thoroughly investigated (e.g. Janowiak 1988, Ropelewski 1988, Namias 1991, Mo et al. 1991, Oglesby and Erikson 1989, Oglesby 1991, Trenberth and Branstator 1992, Atlas et al. 1993). This event was chosen for inter-comparison of nested grid regional models, or PIRCS (Project to Intercompare Regional Climate Simulations) (Takle et al. 1999).

The extensively investigated anomalous regional climate event of the U.S. 1988 summer drought is chosen for this study for testing the developed SG-GCM in the straightforward simulation mode. Our major goal is studying the impact of variable resolution in terms of regional down-scaling rather than producing the case study of the event.

The key objectives of the study are: developing the SG-GCM providing an efficient down-scaling over the area of interest with enhanced fine horizontal resolution, and consistent interactions between regional and global scales; and testing the SG-GCM ability to simulate an anomalous regional climate event.

A description of the GEOS (Goddard Earth Observing System) SG-GCM is presented in Section 2. Section 3 and 4 are devoted to discussing the straightforward simulation results obtained with the SG-GCM for the 1988 summer, for global and regional fields, respectively. The conclusions are given in Section 5.

2. A brief description of the stretched-grid design and the GEOS SG-GCM

a. The stretched-grid design

The stretched-grid used in this study for the GEOS SG-GCM is similar to that of introduced in Staniforth and Mitchell (1978) and used in Fox-Rabinovitz et al.(1997) for the SG-dynamical core experiments (Fig.1). The stretched grid has a uniform (latitude x longitude) fine resolution over the area of interest which has to be a spherical rectangle. Outside the area of interest, the grid intervals are increasing or stretching in both latitudinal and longitudinal directions as a geometric progression with the constant local stretching factor or ratio defined as follows:

$$r_j = dx_j/dx_{j-1} \qquad (1)$$

where dx_j and dx_{j-1} are adjacent grid intervals, and j is the horizontal index.

The total global stretching factor is defined as

$$R = dx_{max}/dx_{min}, \qquad (2)$$

where dxmax and dxmin are the maximal and minimal grid intervals on the sphere, respectively.

Within the portable stretched-grid design, the area of interest, i.e. a uniform fine horizontal resolution spherical rectangle, can be allocated over any part of the globe such as the rectangle over the U.S. used in this study. Note that if the area of interest includes the polar point

or even the vicinity of the pole the stretched grid is to be rotated so that, for example, the polar point will be placed on the equator in the rotated coordinates.

In order to keep under control undesired computational problems arised from grid irregularity, some important properties of the stretched-grid design have to be imposed (Vichnevetsky 1987, Fox-Rabinovitz 1988, Fox-Rabinovitz et al. 1997). First, the stretching should be uniform, i.e. with r_j =3D constant for all j's. Second, the stretching has to be well controlled or moderate in the sense that the local stretching factors should not usually deviate from unity by more than about 10%. This allows one to have very fine mesoscale resolution over the area of interest (e.g. Cote et al. 1993, 1998, Cote 1997) while allocating a significant percentage of the total number of global grid points within the area of interest. This reduces the amount of computations needed over the rest of the globe. Third, to keep the overall accuracy of approximation under control for the moderate stretching strategy mentioned above, the maximal grid intervals have to be not larger than a few (2–4) degrees to be quite close to the resolution of typical GCMs. This is needed for preserving the general integrity or realistic skill of global simulated fields that is necessary for providing consistent interactions between global and regional scales throughout SG-GCM integrations.

It is noteworthy that the strictly controlled SG-parameters needed for the regional climate simulation mode could be relaxed for other modes of integration such as a short-term forecasting (Cote et al. 1993, 1998) and data assimilation modes.

The choice of stretched-grid parameters depends on a particular model design, configuration, requirements, and modes of integration. It also depends on a model's numerical scheme.

The stretched grid used in this study has the same number of grid points as the global uniform 2x2.5 degree grid (UG) but redistributed according to a SG-design (Fig. 1). The 2x2.5 UG-run is used below in Section 4 as a reference run when analyzing the SG-GCM simulation results. The area of interest is the spherical rectangle over the U.S. with 60 km uniform resolution

and the following coordinates: from 25N to 50N and 75W to 125W. For the stretched grid, the local stretching factors (Eq.(1)) are ~7% and ~5% and the total global stretching factors (Eq.(2)) are ~9 and ~8 (that corresponds to the maximal grid intervals of approximately 5 and 6 degrees), for latitudes and longitudes, respectively. The stretched grid has approximately 9 times less grid points than that of the global uniform 60 km resolution grid.

As an option, the spherical grid can be rotated so that the area of interest is located, for example, about the equator in the rotated coordinates (e.g. Takacs et al. 1994). Such a rotation is not necessary for the U.S. region but as it was mentioned above it makes sense for the regions including the pole or located in a close proximity to the pole.

b. A brief description of the GEOS GCM

The GEOS GCM was developed by the Data Assimilation Office (DAO) at the NASA Goddard Laboratory for Atmospheres. The earliest predecessor of the GEOS GCM was developed in 1989 based on the "plug-compatible" concepts outlined in Kalnay et al. (1989). The GCM was subsequently improved in 1991 (Fox-Rabinovitz et al. 1991, Helfand et al. 1991). The Relaxed Arakawa-Schubert cumulus convective parameterization and the re-evaporation of falling rain are based upon the works of Moorthi and Suarez (1992) and Sud and Molod (1988). The long-wave and short-wave radiation is parameterized following Chou and Suarez (1994). The planetary boundary layer and the upper level turbulence parameterizations are based on the level 2.5 closure model of Helfand and Labraga (1988) and Helfand et al. (1991). The orographic gravity wave drag parameterization follows Zhou et al. (1995). The model physics is updated with different frequencies ranging from every two dynamics time steps for turbulence and gravity wave drag, three dynamics time steps for moist processes (convection and large-scale precipitation), to one hour for short-wave and three hours for long-wave radiation. All model physics updates are prorated and applied at every time step.

The momentum equations used in the GEOS GCM are written in the "vector invariant" form, as in Sadourney (1975) and Arakawa and Lamb (1981), to facilitate the derivation of the energy and potential enstrophy conserving 4th-order differencing scheme. The thermodynamic (potential temperature) and moisture (specific humidity) equations are written in flux form to facilitate potential temperature and moisture conservation.The Arakawa C-grid is used for horizontal approximation. For vertical approximation an unstaggered Lorenz (1960) grid in generalized sigma coordinates, is used. The vertical differencing scheme is described in Arakawa and Suarez (1983). The time integration is done with the economical explicit scheme (Ames 1969, Schuman 1971, Brown and Campana 1978, Fox-Rabinovitz 1974), based on a leap-frog scheme with time averaged pressure gradient. The scheme allows one to use approximately twice larger time steps than those of the leap-frog scheme. A complete description of the fourth order finite-difference scheme used in the dynamical core, can be found in Suarez and Takacs (1995).

Since the early 90s, the GEOS GCM is routinely run with 2 x 2.5 degree horizontal resolution and 70 layers in the vertical covering the entire tropospheric and stratospheric domain between the surface and the 0.01 hPa level. The GEOS GCM was developed and used for producing global reanalyses for climate applications. It is also used for long-term simulations such as those of the AMIP (Atmospheric Model Inter-comparison Project).

c. Configurations of the GEOS SG-GCM

At the current stage of the SG-GCM development, a stretched grid is fully implemented into the model dynamical core with real orography as described by Fox-Rabinovitz et al. (1997). Along with introducing a stretched-grid coordinate array, some interpolation techniques depending on a grid definition were modified accordingly. The model filtering procedure has also been modified to account for the changes required for a stretched grid by Fox-Rabinovitz et al. (1997).

The prognostic variables (wind components, temperature, moisture and surface pressure) for the dynamical model state are updated and stored on the model dynamics stretched grid. The diabatic tendencies are updated at the appropriate physical/computational time-scales on their own physical (intermediate uniform) grid. Then they are interpolated, prorated per time step and applied at every time step to the model dynamics stretched grid. Therefore, the whole integration history resides effectively on the stretched grid.

Such an approach is justified by the assumption that model physics and dynamics can have different temporal and spatial resolution. This subject has been discussed by Lander and Hoskins (1997). For a spectral model, they advocate using coarser resolution for model physics than for model dynamics, and further conclude that similar considerations also apply to finite-difference and finite-element models.

At this first stage of the SG-GCM development implementing model physics on an intermediate uniform resolution grid allows us to avoid some potential complications that may arise from calculating all model physics parameterizations on a stretched grid. It was verified that for such a combination of the SG-model dynamics and intermediate uniform grid model physics, the model physics captures ("sees") the finer scale patterns produced by the model dynamics on the stretched grid. Fig.2 shows the instantaneous regional patterns of specific humidity at 850 hPa obtained on the stretched-grid (the upper panel) and interpolated onto the uniform intermediate resolution grid used for model physics calculations(the bottom panel).Both patterns show similar gradients and other features. This similarity takes place because the model dynamics and orographic forcing and the whole integration history resides effectively on the stretched grid.

At the next stage of the model development, the model physics parameterizations will be gradually (one-by-one) implemented on a stretched grid.

Orography is calculated directly on a stretched-grid by averaging, within a grid box, the Navy 1.6 x 1.6 degree surface elevation dataset available from the National Center for Atmospheric Research (NCAR). The grid box averaged orography is passed through a

Lanczos(1966) filter in both dimensions which removes the smallest scales while inhibiting Gibbs phenomena (Takacs et al. 1994).

The stretched grid simulation is compared below to that of a reference run performed with the global uniform 2 x 2.5 degree resolution grid with the same amount of grid points as that of a stretched grid. A strict ultimate validation approach used in this study is comparing the simulated fields against data assimilation, or reanalysis products. It allows us to calculate the mean errors or biases as the deviations of simulated fields from the corresponding verifying analyses.

3. Global seasonal fields for the 1988 summer simulation with the SG-GCM

We start analyzing the results of the SG-GCM simulation with presenting the global model fields for the 1988 summer season (June-July-August, or JJA). In this section, we will focus on discussing the global integrity of simulated fields although the SG-GCM has been developed with the emphasis on regional climate simulation. In the context of regional climate modeling based on the SG-approach, the integrity of global fields is an important property of an SG-GCM simulation. As it was pointed out in the previous Section 2, using a variable-resolution SG-GCM is supposed to provide the appropriate representation of global large scales and their consistent interactions with regional mesoscales.

The SG-GCM integration started at 00Z May 15, 1988 and continued through August 31, 1988. The model prognostic and diagnostic fields are stored every 6 hours and used for producing time-averaged fields. The SG-GCM simulation is run with real surface boundary conditions forcing. Namely, the NCEP monthly mean analyses of soil moisture and weekly mean analyses of SST (sea surface temperature), snow, and sea ice are used. The GEOS DAS reanalysis products produced with the global uniform 2 x 2.5 degree resolution, are used for validation of the SG-GCM simulation.

One of the major goals of the SG-GCM simulation presented in this and the next section is to verify whether the promising results obtained earlier with the SG-dynamical core in the Held-Suarez framework (Fox-Rabinovitz et al. 1997), will be also obtained for the full diabatic SG-GCM. Namely, two major results have to be verified for the SG-GCM simulation: the efficiency of the down-scaling over the area of interest, and the overall "integrity" of global simulated fields.

Let us start discussing the results of the SG-GCM simulation from comparing the obtained seasonal zonal mean vertical distributions for dependent variables against those of the verifying GEOS DAS reanalyses produced for the 1988 summer. The JJA wind component distributions are shown in Fig.3, and those of temperature and relative humidity in Fig.4.

The SG-GCM simulation distributions appear to be quite similar to those of the verifying reanalyses. The position and strength of the jets in both hemispheres are quite well reproduced in the SG-GCM simulation (Fig.3a and b).The Southern Hemisphere jet core (the 40 m/s isoline) is stronger by 10 m/s, larger, and shifted equatorward in the SG-GCM simulation (Figs.3a and 5a) compared to that of of the reanalyses (Fig.3b). The positive bias (or the deviation of the SG-GCM simulation from the verifying GEOS analyses) of 10 m/s in the Southern Hemisphere tropics around the 300–400 hPa layer (Fig.5a), is associated with the equatorward shift of the jet. The larger bias takes place above 100 hPa. All the differences result from coarser resolution within the stretched grid for the Southern Hemisphere. In the better resolved within the stretched grid Northern Hemisphere, the jet position and strength (Fig.3a) are close to those of the reanalyses (Fig. 3b) and the bias (Fig.5a) is smaller, less than 5 m/s, except for the jet core where it is about 5 m/s.

The meridional wind distributions for both the SG-GCM simulation and the GEOS verifying analyses are very close to each other (Figs.3c and d). The similarity takes place in the minima strength (-3.5 m/s) and in both the latitudinal position in the tropics and in the vertical location around 200 hPa. All that indicates that the Hadley cells are also close for both the

simulated and reanalysis fields. The bias in the Northern Hemisphere is small, less than 0.5 m/s. It is a bit bigger, about +/- 0.5 m/s, in the tropics for the 300-100 hPa layer, especially in the Southern Hemisphere, and within the southern polar cap for the lower tropospheric levels (Fig. 5b).

The cold tropical temperature core at the 100 hPa level, the cold polar temperature core above 200 hPa in the Southern Hemisphere, the position of the maximum surface temperature in the Northern Hemisphere tropics (the 295 K degree isoline) as well as the typical gradients, show the overall close pattern similarity for the temperature distributions of the SG-GCM simulation and the verifying reanalyses (Fig.4a and b). The temperature bias (Fig.5c) is less than 3(K for the entire vertical-latitudinal domain, with the exception of the positive (warm) bias of 6(K around the 100 hPa level in the tropics. The larger warm bias up to 12(K is confined to the Southern Hemisphere polar cap and located above the 100 hPa level. Same kind of the overall pattern similarity is obtained for relative humidity including the positions of the maxima near the surface especially in the Northern Hemisphere (Fig.4c and d). The relative humidity bias (Fig.5d) is quite small, mostly within 10-20%, for the entire Northern Hemisphere except for the polar cap around 400 and 200 hPa levels. The bias is also larger, up to 30%, around 50(S at 200 hPa, and up to -25% near the South Pole around 500 hPa.

The horizontal distributions of relative humidity at 850 hPa for the JJA SG-GCM simulation, the verifying reanalysis and their difference or bias, are presented in Fig.6. The simulated and verifying reanalysis fields (Fig. 6a and b) show the close similarity with each other, especially in the Northern Hemisphere. The bias (Fig.6c) over the area of interest and its vicinity is small, mostly 10% and below indicating that the efficient down-scaling takes place for the area. Although the patterns over the Southern Hemisphere are also quite similar (Fig.6a and b) the bias (Fig. 6c) is larger than that of the Northern Hemisphere.

The presented JJA results show that the overall integrity of global fields is preserved, mostly for the better resolved within the stretched grid Northern Hemisphere. The larger bias or

the deviation of the SG-GCM simulation fields from those of the verifying reanalyses for the Southern Hemisphere does not seem to directly negatively affect the results over the area of interest. We also have to realize that some deviations are not related to using the SG-GCM but are inherent to the basic uniform grid GEOS GCM.

4. Regional fields for the 1988 U.S. summer drought simulation with the SG-GCM

In this section, we will discuss the regional fields representing the drought. For analyzing the down-scaling efficiency over the area of interest we compare the SG-GCM and the 2 x 2.5 degree reference UG integrations against the GEOS DAS verifying reanalyses products. For the validation purposes, we will mostly use the June 1988 monthly mean characteristics and also those of the two month drought period from May 15 to July 15, 1988.

The extent of the anomalous drought is shown by the anomaly distributions for June 1988 for the 500 hPa height and total precipitation fields (Fig.7). The anomalies are calculated as the differences between the monthly mean obtained from the GEOS DAS reanalyses and the June climatology. The 1963-1995 climatology is used for calculating the precipitation anomaly (Fig.7a) and that of 1980-1995 for the 500 hPa height anomaly (Fig.7b). The NCEP gauge precipitation for June 1988 is show in Fig.7c.

The strong positive anomaly for the 500 hPa heights over the U.S. and Canada reaching up to 120 m is accompanied by two negative anomalies, one on the east coast and another just off the west coast, both reaching up to -50 m (Fig.7b). The strong negative precipitation anomaly or the drought area is located mostly over the Mississippi River basin reaching up to -2.5 mm/day (Fig.7a). The negative anomaly over the Mississippi River is a strong anomalous regional climate event (e.g. Ropelewski 1988, Janowiak 1988). The more moderate positive rainfall anomaly reaching 1.5-2 mm/day takes place over the south-central part of the U.S. The Midwestern drought area with precipitation less than 1 mm/day is shown in Fig.7c.

a. The 500 hPa height fields

Let us compare the 500 hPa height regional pattern produced by the SG-GCM simulation against the GEOS DAS verifying analyses. The two months mean field obtained from the GEOS DAS (Fig.8d) shows that the anomalous drought event is characterized by a strong ridge over the central part of the U.S. and Canada and by two strong troughs located on the east and west coasts. Such a pattern is consistent with the strong anomaly shown in Fig.7b.

The two months mean 500 hPa height field obtained from the SG-GCM simulation is presented in Fig.8a. It exhibits the major pattern similarity to the GEOS DAS results (Fig.8d). Namely, the SG-GCM simulation (Fig.8a) contains the appropriately positioned ridge and two troughs although the features are less pronounced than those of the verifying analyses (Fig.8d). It seems appropriate to emphasize that this is a positive result for the straightforward two months simulation. To assess it quantitatively, the bias or deviation of the SG-GCM simulation (Fig.8a) from the verifying analyses (Fig.8d) is shown in Fig.8b. The maximum negative bias values reaching -60 m to -80 m are confined to the relatively small area immediately adjacent to the central part of the northern boundary of the area of interest. Over the remaining large part of the area of interest, the bias values are much smaller and are of the different signs. The bias here is mostly within the -20 m to 20 m range. The bias distribution is consistent with but definitely smaller than the June 1988 anomaly (Fig.7b).

The bias for the reference run or the UG-simulation is presented in Fig.8c. It is negative over the entire area of interest and is reaching -110 m. For the large area south of this minimum, the bias is within the -90 m to -50 m range and it is going down to -40 m to -20 m over the remaining part of the area of interest. The overall UG-simulation bias (Fig.8c) is approximately two times larger by magnitude than that of the SG-GCM simulation (Fig.8b) and is comparable with the June 1988 anomaly (Fig.7b). All that shows that the SG-GCM simulation is definitely closer to the verifying analyses than the reference UG-simulation for 500 hPa heights.

We compared the 500 hPa regional verifying analyses with 2x2.5 degree resolution with the newly developed GEOS SG-DAS analyses with 60 km regional resolution. They appeared to produce the similar regional pattern with the same location of the ridge and two troughs as those shown in Fig.8d. The biases produced against these finer resolution analyses are of the same magnitude as shown in Fig.8b.

b. Precipitation

Obtaining the realistic precipitation pattern is evidently the most important goal of the drought simulation. It is also the most difficult field to simulate due to the complexity of the process. Therefore, when analyzing precipitation distributions, we have to concentrate on the major features, with the clear understanding of inevitable limitations of the straightforward two months simulation. The June 1988 monthly mean precipitation fields and biases for June 1988 are presented in Fig.9. The precipitation pattern produced by the GEOS DAS (Fig.9d) shows clearly the drought area for the Mississippi River basin. The minimum (less than 1 mm/day) precipitation area is located in the northern part of the basin. The reduced precipitation occurs over the major part of the Rocky mountains. A stronger precipitation, 2-4 mm/day, is obtained over the south-central, south-eastern and north-western parts of the U.S. This precipitation pattern is consistent with the precipitation anomaly and precipitation pattern shown above (Fig.7a and 7c). It is noteworthy that although the DAS precipitation (Fig.9d) shows some deviations/biases from the NCEP gauge precipitation (Fig.7c) they are located mostly outside of the drought area. They do not seem to affect significantly our discussion of the SG-GCM drought simulation.

The precipitation pattern obtained from the SG-GCM simulation (Fig.9a) shows the minimum with reduced precipitation, below 3 mm/day, over the major drought area, the northern part of the Mississippi River basin. Over the major part of the Rocky mountains, precipitation is reduced. A strong precipitation, up to 4-5 mm/day, takes place over the south-central, eastern and

north-western parts of the U.S. All that makes the precipitation pattern obtained from the SG-GCM simulation, quasi-realistic.

The precipitation biases or deviations calculated against the verifying diagnostics produced by the GEOS DAS, for the SG-GCM simulation and the reference UG-simulation, are presented in Fig.9b and Fig.9c, correspondingly. The SG-GCM simulation bias (Fig.9b) is within the 2-3 mm/day range over the drought area and is definitely smaller than that of the reference UG-simulation ranging there from 3 mm/day to 6 mm/day (Fig.9c). Such a significant bias reduction for the SG-GCM simulation precipitation compared to that of the reference UG-simulation, is an important indication of an efficient down-scaling obtained for this anomalous drought event through the SG-approach.

c. Low level jet

The low level jet (LLJ) makes a significant contribution to the drought formation and sustenance. Its adequate representation is important for a successful regional climate simulation of the anomalous event.

The 925 hPa monthly mean wind vectors for June 1988 representing the LLJ for the SG-GCM simulation, the reference UG-simulation, and for the verifying GEOS DAS reanalyses, are shown in Fig.10. According to the verifying analyses (Fig.10c), the southeastern flow approaching Texas from the Gulf of Mexico gradually turns clockwise. It becomes a predominantly southern flow east of the Rocky mountains or over the western part of the Mississippi River basin. Over the central and eastern part of the basin, the flow is weak.

Such a pattern is basically well reproduced in the SG-GCM simulation (Fig.10a). The southeastern flow over the Gulf of Mexico turns clockwise and becomes the southern flow over Texas and east of the Rocky Mountains, with both the direction and intensity similar to those of the verifying analyses (Fig.10c). The weak flow over the central and eastern part of the Mississippi River basin (Fig.10a) is also similar to that of the verifying analyses Fig.10c). Even

outside the area of interest for the immediate vicinity of the U.S., the SG-GCM simulation wind velocity is quite similar to that of the verifying analyses, with the exception of the flow over the central and eastern Canada.

However, the LLJ pattern for the reference UG-simulation (Fig.10b) is completely different from that of the verifying analyses (Fig.10c) over the drought area. There is no southern flow located east of the Rocky mountains. Instead, the southeastern flow coming from the Gulf of Mexico to Texas turns westward. As the result, the strong westerlies flow throughout the entire drought area and further east. Such a LLJ pattern for the reference UG-simulation (Fig.10b) appears to be not as realistic as that of the SG-GCM simulation (Fig.10a).

Let us consider now the diurnal LLJ variations. The nocturnal LLJ is characterized by the maximum winds taking place around 3-5 a.m. (local time). To show the diurnal variations, the monthly mean wind vectors are calculated for 00Z and 12Z. These 00Z and 12Z monthly means are overlapped for comparison purposes, and presented in Fig.11. The overlapped wind vectors are "v"-shaped for the southeastern flow comings from the Gulf of Mexico to the western part of the drought area. The right "v"-branch corresponds to the 12Z monthly means and the left "v"-branch to the 00Z monthly means. For the area of the drought, 12Z corresponds to ~5 a.m. local time for which the nocturnal LLJ winds are supposed to be stronger than those of 00Z or ~5 p.m. local time.

The wind vectors obtained from the verifying analyses (Fig.11b) for the LLJ east of the Rocky mountains, are rotated clockwise from the left 00Z "v"-branch to the right 12Z "v"-branch. The right 12Z "v"-branches are mostly longer than the 00Z ones that is appropriate for the nocturnal LLJ. This major feature as well as the above clockwise rotation are well reproduced in the SG-GCM simulation (Fig.11a). The whole pattern for the SG-GCM simulation is quite similar to that of the verifying analyses (Fig.11a and b). The pattern and the above features over the area of the drought for the reference UG-simulation (not shown), with the dominating westerlies over

the drought area (Fig.10b), are significantly different from those of the verifying analyses (Fig.11b).

One of the plausible explanations for the differences between the LLJ patterns obtained for the SG-GCM simulation and the UG-simulation, could be the fact that orography is better resolved for the stretched grid than for the UG within the area of interest. As the result, the SG-mountains are producing stronger blocking effects for the flow coming from the Rocky mountains into the drought area. The weaker blocking effects for the UG-simulation result in strong westerlies developing over the drought area that is not supported by the verifying analyses.

Similar results consistently favorable to the SG-GCM simulation vs. the UG-simulation are obtained for other model fields and diagnostics.

d. Extended simulation and down-scaling effects

The SG-GCM simulation was extended to one year to verify whether the positive down-scaling effects discussed above will persist in longer integrations. This is an important issue for potential applications of the SG-approach to long-term climate and climate change regional assessments.

The extended simulation results are presented for the winter season or DJF (December 1988, January and February 1989). Note that the qualitatively similar results are obtained for the fall of 1988 and the spring of 1989. The overall integrity of global fields for DJF is similar to that of JJA presented in Section 3. We will focus here on discussing the regional down-scaling aspects for DJF.

The DJF LLJ for the SG-GCM simulation and the reference UG-run are compared against the verifying GEOS DAS analyses in Fig.12. The LLJ for the SG-GCM simulation (Fig.12a) and the verifying analyses (Fig.12c) are close to each other. Both patterns contain strong southern flow coming from Gulf of Mexico. The UG-run has failed to represent this important feature and shows only the westerlies prevailing over the region east of the Rocky

Mountains (Fig.12b). The prognostic variable biases for different model levels are consistently smaller for the major part of the region by approximately 30%–40% for the SG-GCM simulation compared to those of the UG-run. The biases for 850 hPa temperatures are presented in Fig.13. The SG-GCM simulation has smaller biases (Fig.13a) than those of the UG-run (Fig.13b) for the region east of the Rocky Mountains.

To continue the bias discussion we present the global zonal mean DJF biases calculated against verifying analyses, for the 925 hPa meridional winds and 850 hPa specific humidity for the SG-GCM simulation and the UG-run (Fig.14). Over the region of interest (125W to 75W) the SG-GCM simulation biases are predominantly smaller than those of the UG-run. Outside of the area of interest, the UG-run biases are mostly smaller. The SG-biases in the S. Hemisphere depend on coarser resolution within the stretched grid compared to those of the better resolved N. Hemisphere. All that shows the significant dependence on local/regional resolution for the SG-GCM simulation.

The legitimate question to ask concerning the better skill SG-GCM simulation whether the efficient down-scaling to mesoscales will be seen in seasonal mean fields. In other words, will time averaging filter out all the mesoscale structures produced in the course of integration or they are persistent enough to affect seasonal time scales? The 925 hPa DJF vorticity fields for the SG-GCM simulation and the UG-run are presented in Fig.15. The mesoscale structures are produced for the SG-GCM simulation over the Appalachians and the rest of the region east of the Rocky Mountains (Fig.15a). Only synoptic scale features are produced for the UG-run (Fig.15b). Because of the better regional climate skill for the SG-GCM simulation we conclude that the down-scaling is efficient in the sense that introducing enhanced regional resolution resulted in better regional simulation results.

5. Conclusions

The developed SG-GCM is the new tool for producing enhanced resolution regional (not global) climate simulations. The hypothesis verified in this paper is whether the potentially positive impact of finer enhanced resolution provided for prognostic fields within a stretched grid over the region of interest, can counteract the potentially negative impact of a relatively poorly resolved flow coming into the region. Actually, a "working compromise" not a "perfect solution" is sought for the region of interest when applying the SG-approach to regional climate modeling. The results obtained in the study show that the developed SG-GCM provides such a "working compromise" so that the SG-GCM regional fields are closer to the verifying analyses than those of the reference UG-run. Also, the efficient down-scaling to mesoscales is obtained over the region of interest for the SG-GCM simulation.

The following conclusions are arrived at as the result of the study.

1. The variable resolution stretched-grid modeling approach is introduced to the GEOS GCM with finite-difference dynamics for the regional climate simulation mode. The variable resolution stretched-grid version of the fully diabatic GCM is developed and successfully tested in the simulation mode.
2. The straightforward continuous (with no updates) stretched-grid GCM simulation with 60 km regional resolution is performed for the 1988 summer. The seasonal global fields show the overall global integrity that is necessary for an adequate representation of consistent interactions between global and regional scales.
3. The stretched-grid GCM simulation of the anomalous climate event of the 1988 U.S. summer drought shows the efficient down-scaling over the region of interest. The SG-GCM simulation results are significantly closer to those of the verifying analyses than the results of the reference experiment with the global 2 x 2.5 degree uniform grid with the same amount of grid points as for the stretched grid.

4. The major drought characteristics such as precipitation, the 500 hPa height pattern, and the LLJ, are successfully represented in the stretched-grid GCM simulation.
5. Similar positive down-scaling effects are obtained for the extended to one year simulation. It shows that the SG-approach is valid for long-term regional climate simulation and related applications.
6. The obtained results show that the stretched-grid approach is a viable candidate for regional climate simulation studies and applications.

Acknowledgments. The authors would like to thank Dr. A. Staniforth, Prof. A. Arakawa, and Dr. A. Kasahara for productive discussions, and Ms. M. Hall for typing the manuscript. The study has been supported by NASA Grant 578-41-11-20 and the DOE Grant DE-FG02-98ER62618. The authors would like to thank Dr. Kenneth Bergman, the NASA Program Manager, and Dr. Jerry Elwood, the DOE Program Manager, for their support of the study.

References

Ames, W. F., 1969: Numerical methods for partial differential equations. London, Nelson, 291 pp.

Arakawa, A. and V. R. Lamb, 1981: A potential enstrophy and energy conserving scheme for the shallow water equations. *Mon. Wea. Rev.*, **109**, 18-36.

Arakawa, A. and M. J. Suarez, 1983: Vertical differencing of the primitive equations in sigma coordinates. *Mon. Wea. Rev.*, **111**, 34-45.

Atlas, R., N. Wolfson and J. Terry, 1993: The effect of SST and soil moisture anomalies on GLA model simulations of the 1988 US summer drought. *J. Climate*, **6**, 2034-2048.

Brown, J. A., and K. Campana, 1978: An economical time differencing scheme for numerical weather prediction. *Mon. Wea. Rev.*, **106**, 1125-1136.

Caya D., and R. Laprise, 1999: A semi-implicit semi-Lagrangian regional climate model: The Canadian RCM. *Mon. Wea. Rev.*, **127**, 341-362.

Chou M.-D., and M. J. Suarez, 1994: An efficient thermal infrared radiation parameterization for use in GCMs. NASA Tech. Memo. 104606, v.3, 85 pp. [Available from NASA/GSFC, Data Assimilation Office, Greenbelt, MD 20771].

Cote J., M. Roch, A. Staniforth, and L. Fillion, 1993: A variable-resolution semi-Lagrangian finite-element global model of the shallow-water equations. *Mon. Wea. Rev.*, **121**, 231-243.=20

Cote, J., 1997: Variable resolution techniques for weather prediction. *Meteor. Atmos. Phys.*, **63**, 31-38.

Cote, J., S. Gravel, A. Methot, A. Patoine, M. Roch, and A. Staniforth, 1998: The operational CMC/ MRB Global Environmental Multiscale (GEM) model. Part 1: Design Considerations and Formulation. *Mon. Wea. Rev.*, **126**, 1373-1395.

Courtier, P., and J.-F.Geleyn, 1988: A global numerical weather prediction model with variable resolution: application to the shallow-water equations. *Q. J. Roy. Met. Soc.*, **114**, 1321-1346.=20

Deque, M., and J. P. Piedelievre, 1995: High resolution climate simulation over Europe. *Climate Dynamics*, **11**, 321-339.

Dickinson, R. E., R. M. Errico, F. Giorgi, G. T. Bates, 1989: A regional climate model for the Western United States. *Clim. Change*, **15**, 383-422.

Fox-Rabinovitz, M. S., 1974: Economical explicit and semi-implicit integration schemes for forecast equations. *Sov. Met. Hydrol.*, **11**, 11-19.

Fox-Rabinovitz, M. S., 1988: Dispersion properties of some regular and irregular grids used in atmospheric models. Proc. 8th Conf. on Numerical Weather Prediction. Baltimore, AMS, 784-789.

Fox-Rabinovitz, M., H. M. Helfand, A. Hou, L. L. Takacs, and A. Molod, 1991: Numerical experiments on forecasting, climate simulation and data assimilation with the new 17 layer GLA GCM. Ninth Conference on Numerical Weather Prediction. 21-25 October 1991, Denver, CO, 506-509.

Fox-Rabinovitz, M. S., L. V. Stenchikov, M. J. Suarez, L. L. Takacs, 1997: A finite-difference GCM dynamical core with a variable resolution stretched-grid. *Mon. Wea. Rev.*, Vol. 125, No. 11, 2943-2968.

Giorgi, F., 1990: Simulation of regional climate using a limited area model nested in a GCM. *J. Climate*, 3, 941-963.

Giorgi, F., 1995: Perspectives for regional earth system modeling. *Global and Planetary Change*, 10, 23-42.

Janowiak, J. E., 1988: The global climate for March - May 1988: The end of the1986-87 pacific warm episode and the onset of widespread drought in the United States. *J. Climate*, 1, 1019-1040.

Juang, H.-M. H., and M. Kanamitsu, 1994: The NMC nested regional spectral model. *Mon. Wea. Rev.*, **122**, 3-26.

Hardiker, V., 1997: A global numerical weather prediction model with variable resolution. *Mon. Wea. Rev.*, **125**, 349-360.

Held, I. M., and M. J. Suarez, 1994: A benchmark calculation for the dry dynamical cores of atmospheric general circulation models. *Bull. Amer. Meteor. Soc.*, **75**, 1825-1830.

Harshvardhan, R. Davies, D. A. Randall, and T. G. Corsetti, 1987: A fast radiation parameterization for atmospheric circulation models. *J. Geophys. Res.*, **92**, 1009-1016.

Helfand, H. M., and J. C. Labraga, 1988: Design of a non-singular level 2.5 second-order closure model for the prediction of atmospheric turbulence. *J. Atmos. Sci.*, **45**, 113-132.

Helfand, H. M., M. Fox-Rabinovitz, L. Takacs, and A. Molod, 1991: Simulation of the planetary boundary layer and turbulence in the GLA GCM. Proceedings of the AMS Ninth Conference on Numerical Weather Prediction, 21-25 October 1991, Denver, CO, 514-517.

Higgins, R. W., Y. Yao, and J. Wang, 1997: Influence of North American monsoon system on the U.S. summer precipitation regime. *J. Climate*, **10**, 2600-2622.

Kalnay, E., M. Kanamitsu, J. Pfaendtner, J. Sela, M. Suarez, J. Stackpole, J. Tuccillo, L. Umscheid, and D. Williamson, 1989: Rules for the interchange of physical parameterizations. *Bull. Am. Met. Soc.*, **70**, 620-622.

Lanczos C., 1966: Discourse of Fourier Series. Hafner Publishing, New York, 255 pp.

Lander, J., and B.J. Hoskins, 1997: Believable scales and parameterizations in a spectral model. *Mon. Wea. Rev.*, **125**, 292-303.

Lau, K.-M. and L. Peng, 1992: Dynamics of atmospheric teleconnections during the northern summer. *J. Climate*, **5**, 140-158.

Lindzen, R. S., and M. S. Fox-Rabinovitz, 1989: Consistent vertical and horizontal resolution. *Mon. Wea. Rev.*, 117, No. 11, 2575-2583.

Lorenz, E. N., 1960: Energy and numerical weather prediction. *Tellus*, **12**, 364-373.

McGregor, J. L., and J. J. Katzfey, 1998: Simulating typhoon recurvature with a variable resolution conformal-cubic model. In Research Activities in Atmospheric and Oceanic Modeling, Report No.28 (ed. H.Ritchie), WMO/TD-No.942, 3.19-3.20.

Mo, D. C., J. R. Zimmerman, E. Kalnay and M. Kanamitsu, 1991: A GCM study of the 1988 United States drought. *Mon. Wea. Rev.*, **119**, 1512-1532.

Moorthi, S., and M. J. Suarez, 1992: Relaxed Arakawa Schubert: A parameterization of moist convection for general circulation models. *Mon. Wea. Rev.*, **120**, 978-1001.

Namias, J., 1991: Spring and summer 1988 drought over the contiguous United States - Causes and prediction. *J. Climate*, **4**, 54-65.

Oglesby, R. J. and D. Erikson, 1989: Soil moisture and persistence of North American drought. *J. Climate*, **2**, 1362-1380.

Oglesby, R. J., 1991: Springtime soil moisture, natural climatic variability and North American drought as simulated by the NCAR Community Climate Model. *J. Climate*, **4**, 890-897.

Oliger, J., and A. Sundstrom, 1978: Theoretical and practical aspects of some initial boundary value problems in fluid dynamics. *S.I.A.M. J. Appl. Math.*, **35**, 419-446.

Paegle, J., 1989: A variable resolution global model based upon Fourier and finite-element representation. *Mon. Wea. Rev.*, **117**, 583-606.

Pan, Z., E. Takle, W. Gutowski, and R. Turner, 1999: Long simulation of regional climate as a sequence of short segments. *Mon. Wea. Rev.*, **127**, 308-321.

Pielke, R. A., W. R. Cotton, R. L. Walko, C. J. Tremback, W. A. Lyons, L. D. Grasso, M. E. Nicholls, M. D. Moran, D. A. Wesley, T. J. Lee and J. H. Copeland, 1992: A comprehensive meteorological modeling system - RAMS. *Meteor. Atmos. Phys.*, **49**, 69-91.

Qian, J.-H., F. Semazzi, and J. Scroggs, 1998: A global non-hydrostatic semi-Lagrangian atmospheric model with orography. *Mon. Wea. Rev.*, **126**, pp. 747-771.

Ropelewski, C. H., 1988: The global climate for June - August 1988: A swing to the positive phase of the southern oscillation, drought in the United States, and abundant rain monsoon areas. *J. Climate*, **1**, 1153-1174.

Roads, J. O., S.-C. Chen, A. K. Guetter and K. P. Georgakakos, 1994: Large scale aspects of the United States hydrologic cycle. *Bull. Amer. Meteor. Soc.*, **75**,1589-1610.

Sadourney, R., 1975: The dynamics of finite difference models of the shallow water equations. *J. Atmos. Sci.*, **32**, 680-689.

Schmidt, F., 1977: Variable fine mesh in a spectral global model. *Beit. Phys. Atmos.*, **50**, 211-217.

Schuman, F. G., 1977: Resuscitation of an integration procedure. NMC Office Note 54, 55 pp. [Available from NCEP/NOAA, 5200 Auth Road, Camp Springs, MD 20746.]

Semazzi, F. H. M., J.-H. Qian, and J. S. Scroggs, 1995: A global non-hydrostatic semi-Lagrangian atmospheric model. *Mon. Wea. Rev.*, **123**, pp. 2534-2550.

Staniforth, A., 1995: Regional modeling: theoretical discussion, WMO PWPR Report Series, No. 7. WMO/TD-No. 699, 9-18.

Staniforth, A., and H. Mitchell, 1978: A variable resolution finite element technique for regional forecasting with primitive equations. *Mon. Wea. Rev.*, 106, 439-447.

Staniforth, A., 1997: Regional modeling: A theoretical discussion. *Meteorology and Atmospheric Physics*, **63**, 15-29.

Staniforth, A.N., and R. Daley, 1979: A baroclinic finite element model for regional forecasting with the primitive equations. *Mon. Wea. Rev.*, **107**, 107-121.

Suarez, M. J., and L. L. Takacs, 1995: Documentation of the Aries/GEOS Dynamical Core Version 2. NASA Tech. Memo. 104606, NASA, Goddard Space Flight Center, Greenbelt, MD, 103 pp.

Sud, Y. C., and A. Molod, 1988: The roles of dry convection, cloud-radiation feedback processes and the influence of recent improvements in the parameterization of convection in the GLA GCM. *Mon. Wea. Rev.*, **116**, 2366-2387.

Takacs, L. L., A. Molod, and T. Wang, 1994: Goddard Earth Observing System (GEOS) General Circulation Model (GCM) Version 1. NASA Tech.Memo. 104606, v.1, NASA, Goddard Space Flight Center, Greenbelt, MD, 97 pp.

Takacs, L. L., and M. J. Suarez, 1996: Dynamical aspects of climate simulations using the GEOS GCM. NASA Tech. Memo. 104606, v. 10, 56pp.

Takle, E. S., and co-authors, 1999: Project to intercompare regional climate simulations (PIRCS): Description and initial results. *J. Geophys. Res.*, submitted.

Trenberth, K. E., and G. W. Branstator, 1992: Issues in establishing causes of the 1988 drought over North America. *J. Climate*, **5**, 159-172.

Trenberth, K. E., G. W. Branstator and P. A. Arkin, 1988: Origins of the 1988 North American drought. *Science*, **242**, 1640-1645.

Vichnevetsky, R., 1987: Wave propagation and reflection in irregular grids for hyperbolic equations. *Appl. Numer. Math.*, North Holland, v. 2, No. 1-2, 133-166.

Yeh, K.-S., J. Cote, S. Gravel, A. Patoine, M. Roch, A. Methot, and A. Staniforth, 1999: The non-hydrostatic GEM model. WMO/CAS/JSC/WGNE Research Activities in Atmospheric and Oceanic Modeling. Rep. No. 28 (ed. H.Ritchie). WMO/TD-No.942, 5.58-5.59.

Yessad, K.,and P.Benard, 1996: Introduction of local mapping factor in the spectral part of the Meteo-France global variable mesh numerical forecast model. *Quart. J. Roy. Meteor. Soc.*, **122**, 1701-1719.

Zhou, J., Y.C. Sud, and K.-M. Lau, 1995: Impact of orographically induced gravity wave drag in the GLA GCM, *Quart. J. Roy. Meteor. Soc.*, 122, 903-927.

Figure captions

Fig.1 The stretched grid with the area of interest over the U.S.

Fig.2 Instantaneous fields of the 850 hPa specific humidity (SPHU-850) for (a) the SG-GCM simulation with 60 km regional resolution produced by model dynamics and (b) the same field interpolated onto an intermediate uniform resolution grid used for calculating model physics. The contour interval is 1 g/kg.

Fig.3 Seasonal (JJA) wind component zonal-vertical distributions for: (a) U-wind for the SG-GCM simulation; (b) U-wind for the GEOS DAS reanalyses; (c) V-wind for the SG-simulation; (d) V-wind for the GEOS DAS reanalyses. The contour intervals are 5 m/s for (a) and (b); and 0.5 m/s for (c) and (d).

Fig.4 Same as in Fig.3 but for temperature, (a) and (b), and relative humidity, (c) and (d). The contour intervals are 5 K degrees for (a) and (b) and 10% for (c) and (d).

Fig.5 Seasonal (JJA) zonal-vertical bias distributions or the deviations of the SG-GCM simulation fields from the the GEOS DAS reanalyses (both shown in Figs. 3 and 4) for: (a) U-wind; (b) V-wind; (c) temperature; and (d) relative humidity. The contour intervals are 5 m/s for (a), 0.5 m/s for (b); 3(K for (c); and 5% for (d).

Fig.6 Seasonal (JJA) horizontal distributions of relative humidity at 850 hPa for: (a) the SG-GCM simulation; (b) the GEOS DAS reanalyses; and (c) the bias or differences between (a) and (b). The contour intervals are 10%.

Fig.7 (a) Precipitation (b) 500 hPa height anomalies, and (c) NCEP gauge precipitation for June 1988. The contour intervals are 0.5 mm/day for (a), 10 m for (b), and 1 mm/day for (c).

Fig.8 The two month mean (May 15 to July 15, 1988) 500 hPa heights for: (a) the SG-GCM simulation; (b) the SG-GCM simulation bias; (c) the reference UG-simulation bias; (d) the verifying GEOS DAS analyses. The contour interval is 40 m for (a) and (d); and 20 m for (b) and (c).

Fig.9 Same as in Fig.8 but for monthly mean (June 1988) precipitation. The contour interval is 1 mm/day.

Fig.10 The monthly mean (June 1988) wind vectors for the 925 hPa level or LLJ for: (a) the SG-GCM simulation; (b) the reference UG-simulation; (c) the verifying GEOS DAS reanalyses.

Fig.11 The 00Z and 12Z monthly mean (June 1988) wind vectors (overlapped) for the 925 hPa level for: (a) the SG-GCM simulation; (b) the verifying GEOS DAS reanalyses.

Fig.12. The seasonal DJF (December 1988-January-February 1989) mean wind vectors for the 925 hPa level or LLJ for: (a) the extended SG-GCM simulation; (b) the extended UG-simulation; (c) the verifying GEOS DAS reanalyses.

Fig.13. The seasonal DJF 850 hPa temperature biases calculated against the GEOS DAS verifying analyses for: (a) the extended SG-GCM simulation; and (b) the extended UG-simulation. The contour interval is 0.5 degree K.

Fig.14. The DJF zonal mean biases calculated against the GEOS DAS verifying analyses for the extended SG-GCM simulation (open circles) and the extended UG-run (dark circles) for: (a) the 925 hPa meridional wind (V-925); and (b) the 850 hPa specific humidity (SPHU-850). The units are m/sec and g/kg for the meridional wind and specific humidity, correspondingly.

Fig.15. The seasonal DJF 925 hPa vorticity for: (a) the extended SG-GCM simulation; and b) the extended UG-simulation. The contour interval is 10^{-5} s^{-1}.

90N
60N
30N
EQ
30S
60S
180
120W
60W
0
60E
120E
NW
NE
SW
SE

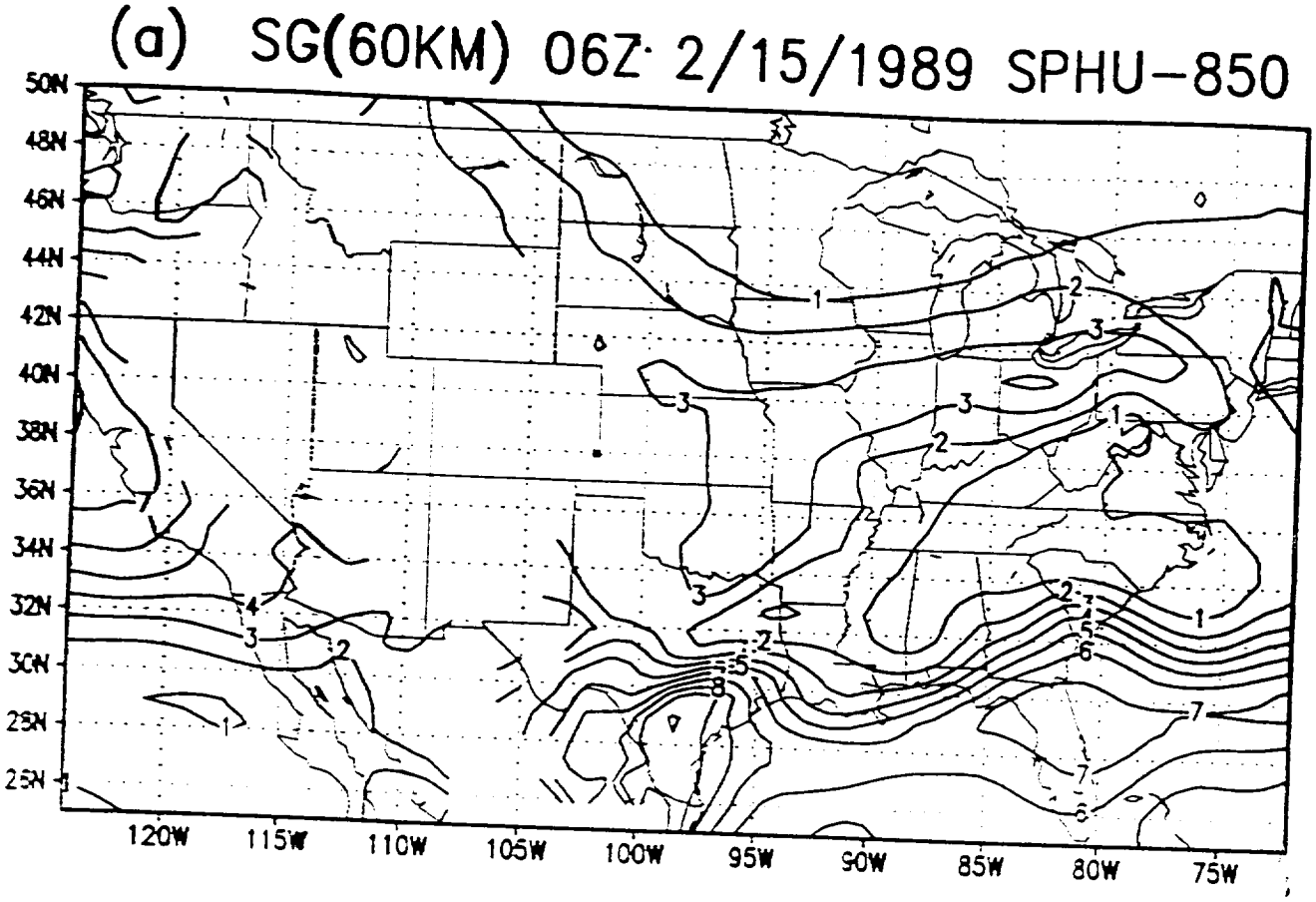
(a) SG(60KM) 06Z 2/15/1989 SPHU-850
50N
48N
46N
44N
42N
40N
38N
36N
34N
32N
30N
28N
26N
120W
115W
110W
105W
100W
95W
90W
85W
80W
75W

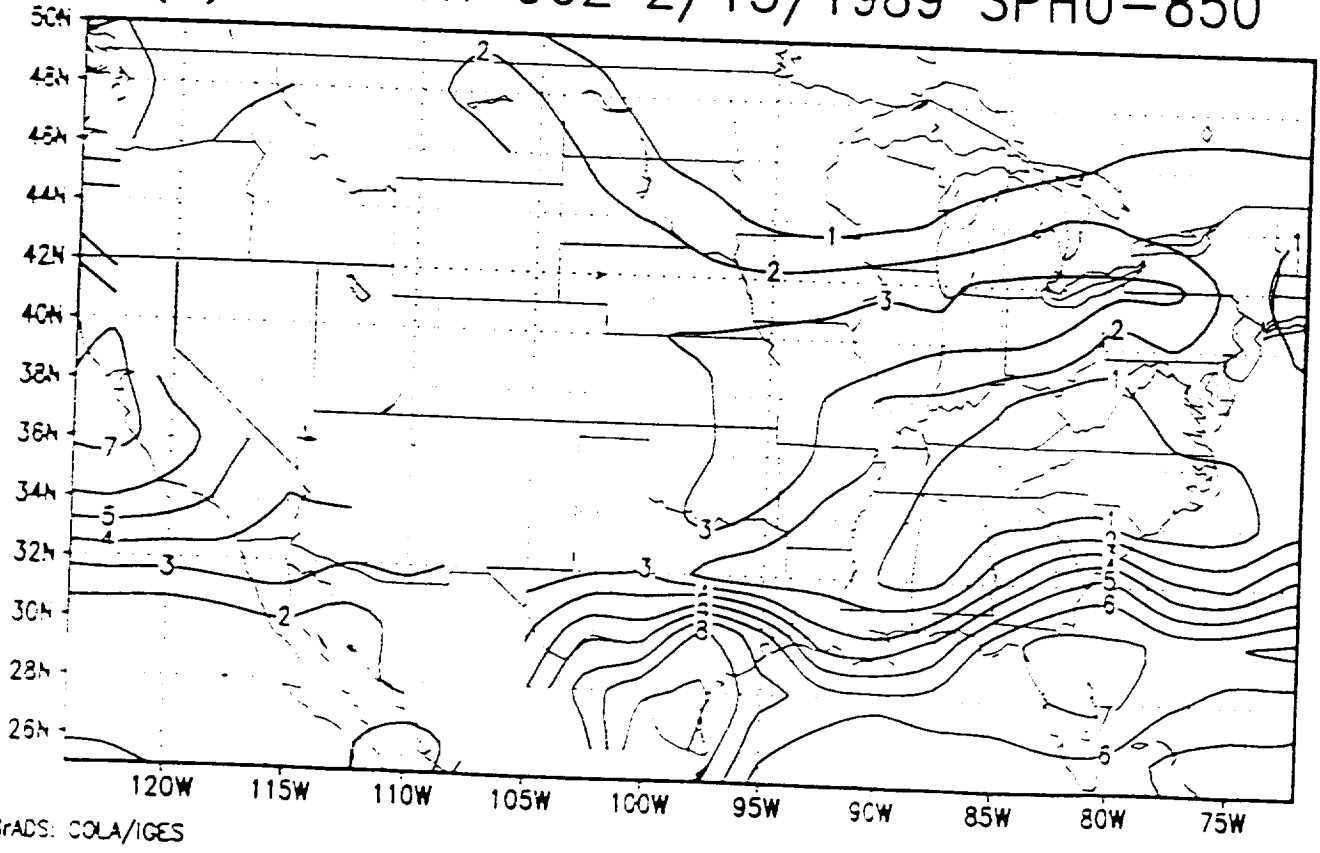
(b) SG-INT 06Z 2/15/1989 SPHU-850
42N
40N
38N
36N
34N
32N
30N
28N
26N
120W
115W
110W
105W
100W
95W
90W
85W
80W
75W
GrADS: COLA/IGES

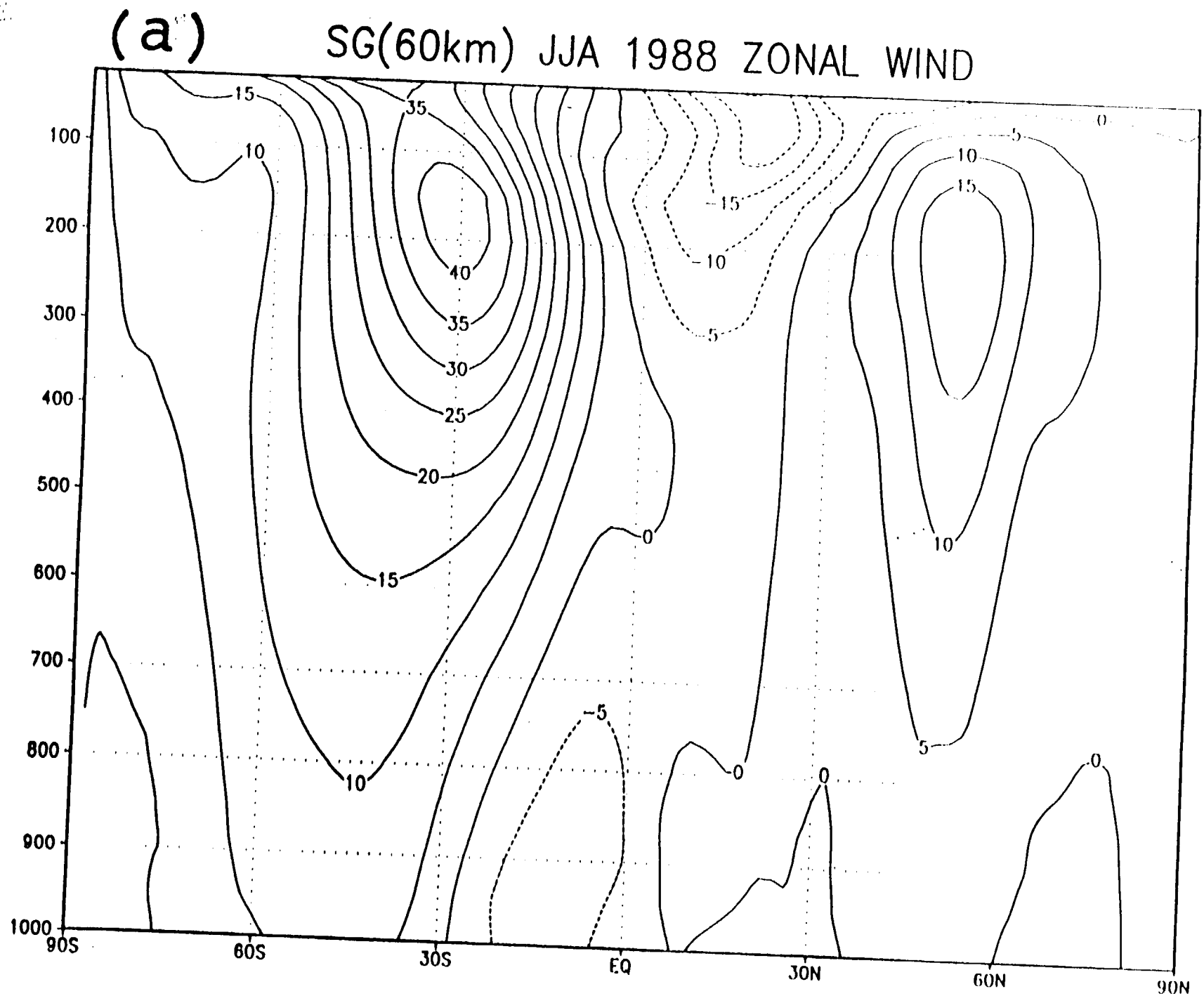

GrADS: COLA/IGES

1999 05 21 11:19

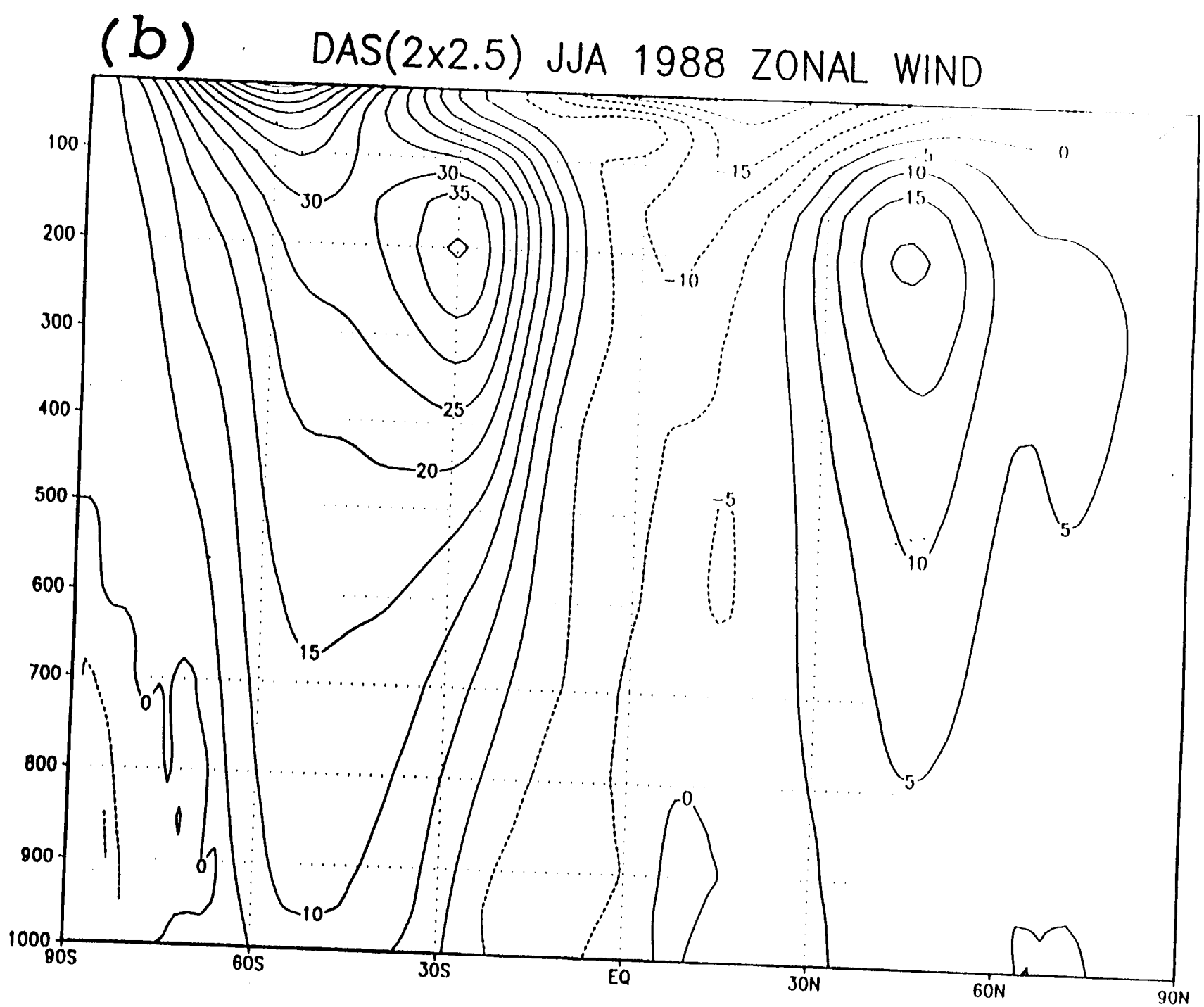

GrADS: COLA/IGES

1999-05-21-10:39

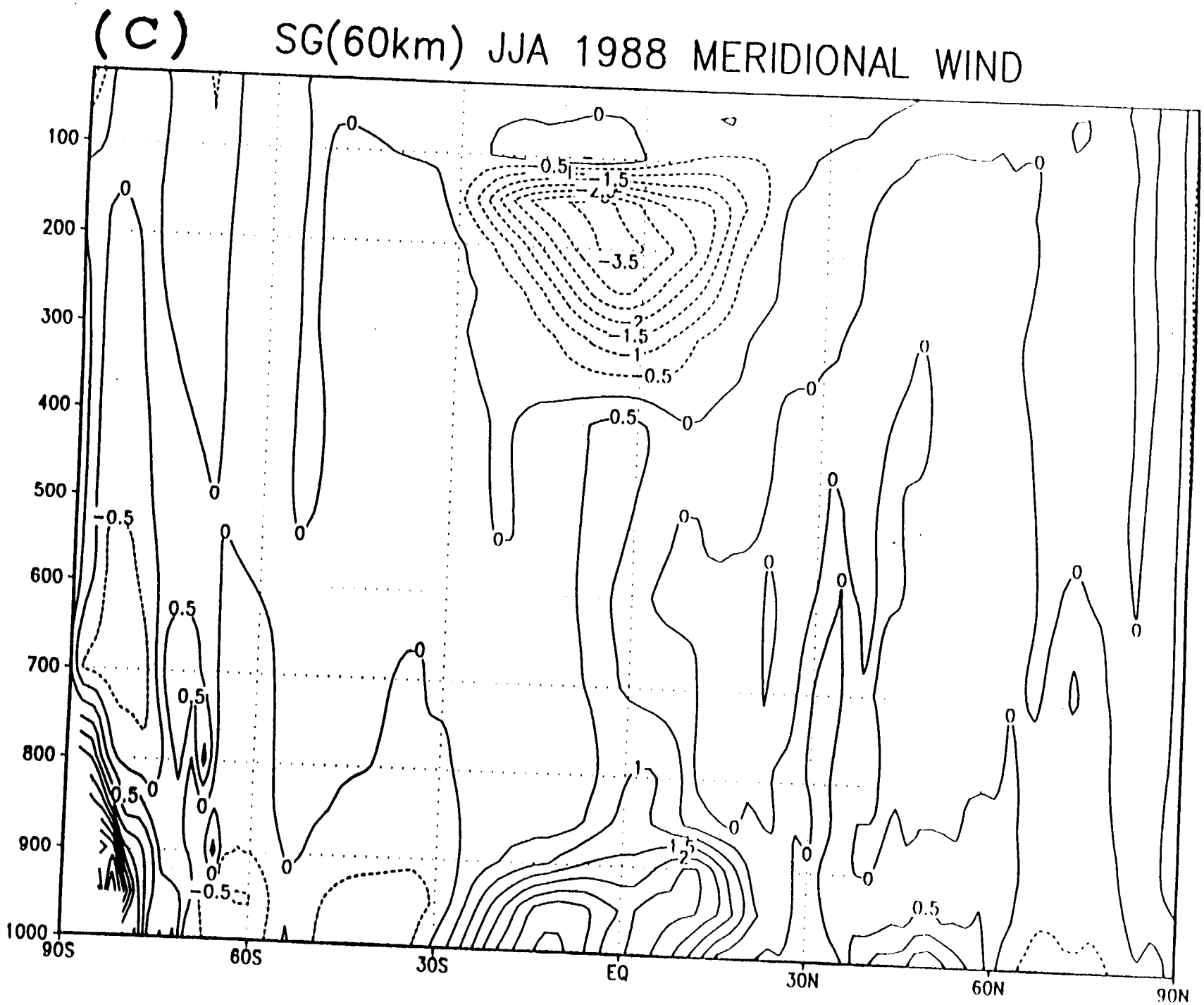

GrADS: COLA/IGES

1999-05-21 11:20

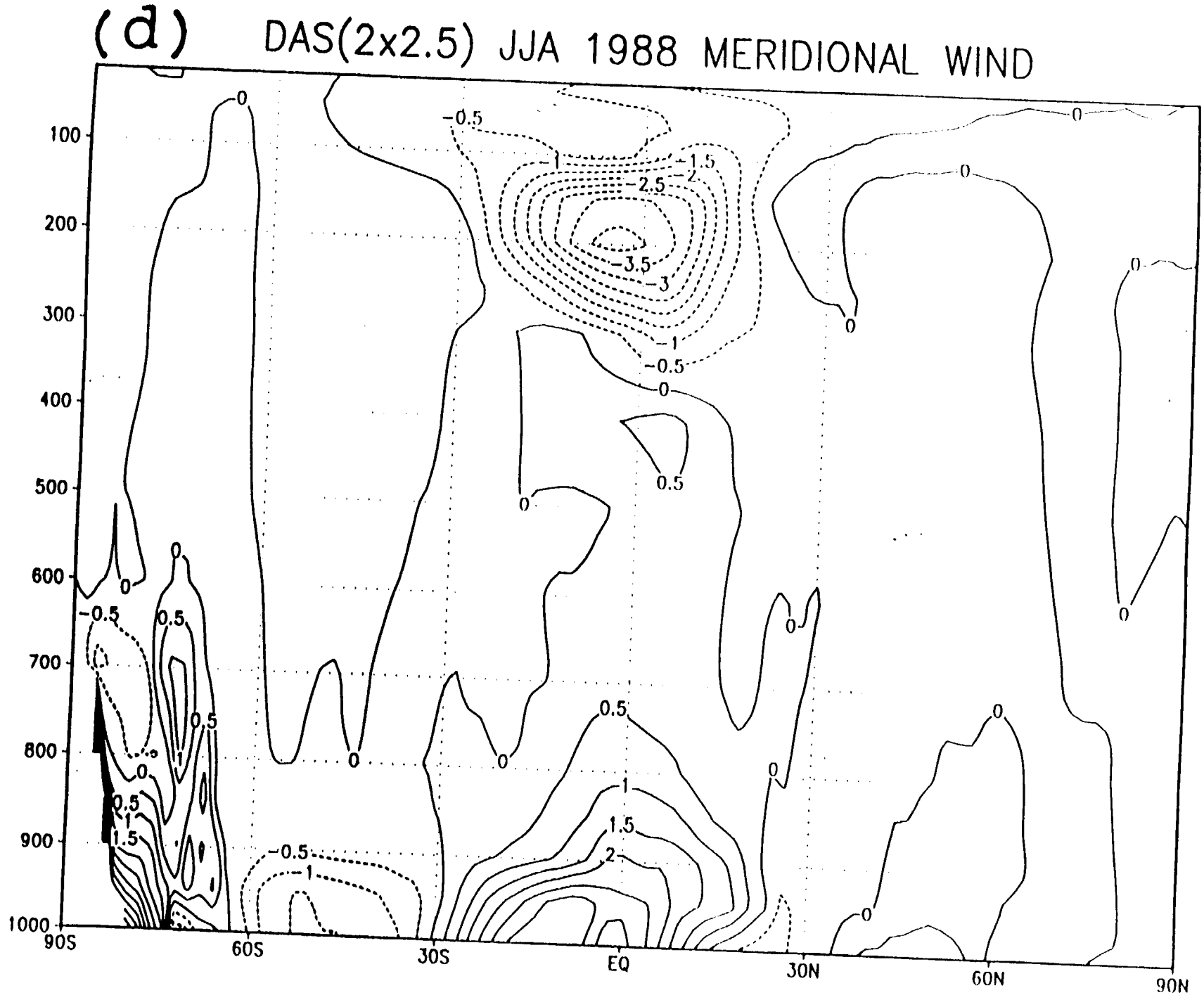

GrADS: COLA/IGES

1999 05 21 10:40

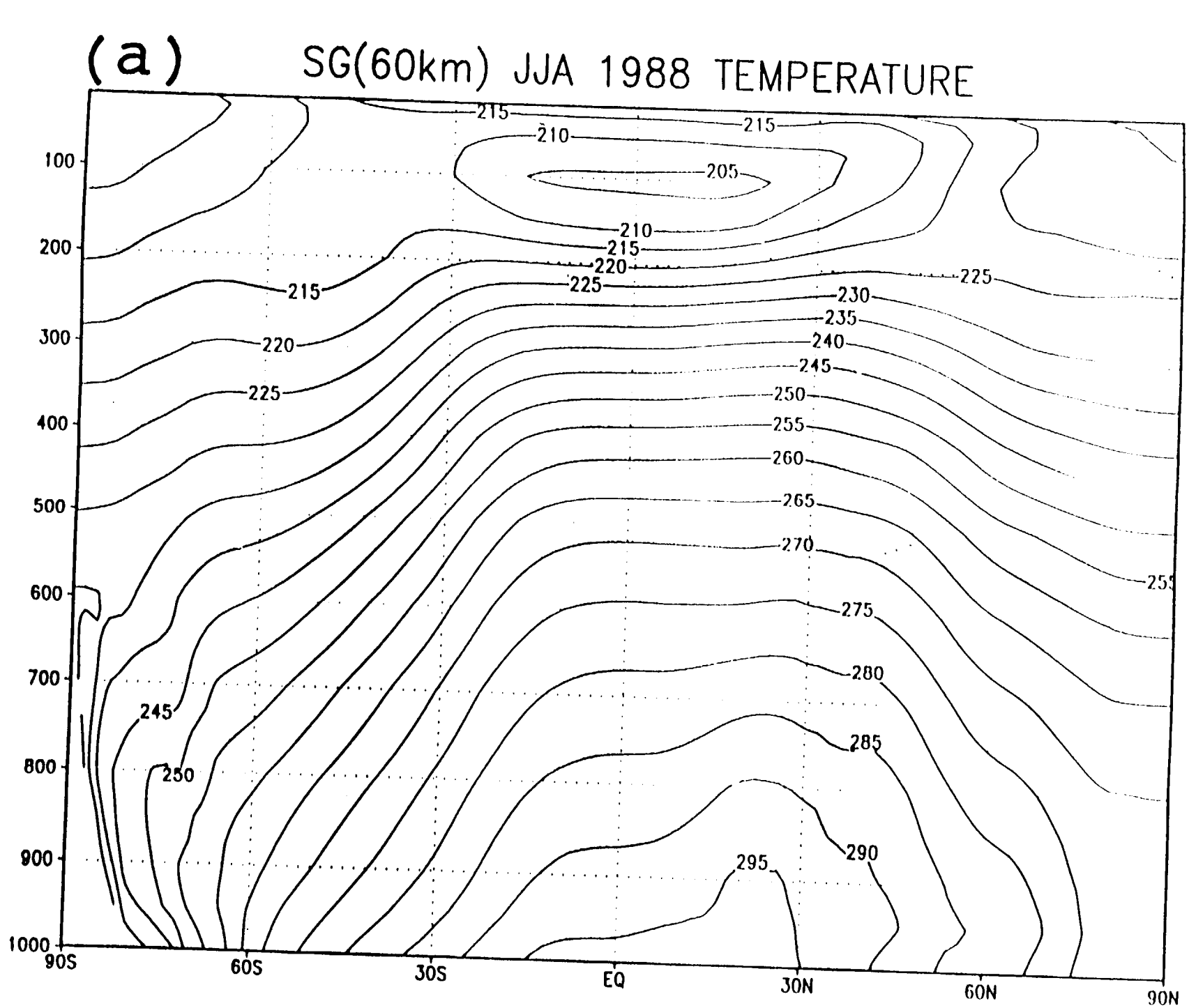

GrADS: COLA/IGES

1999 05 21 11:21

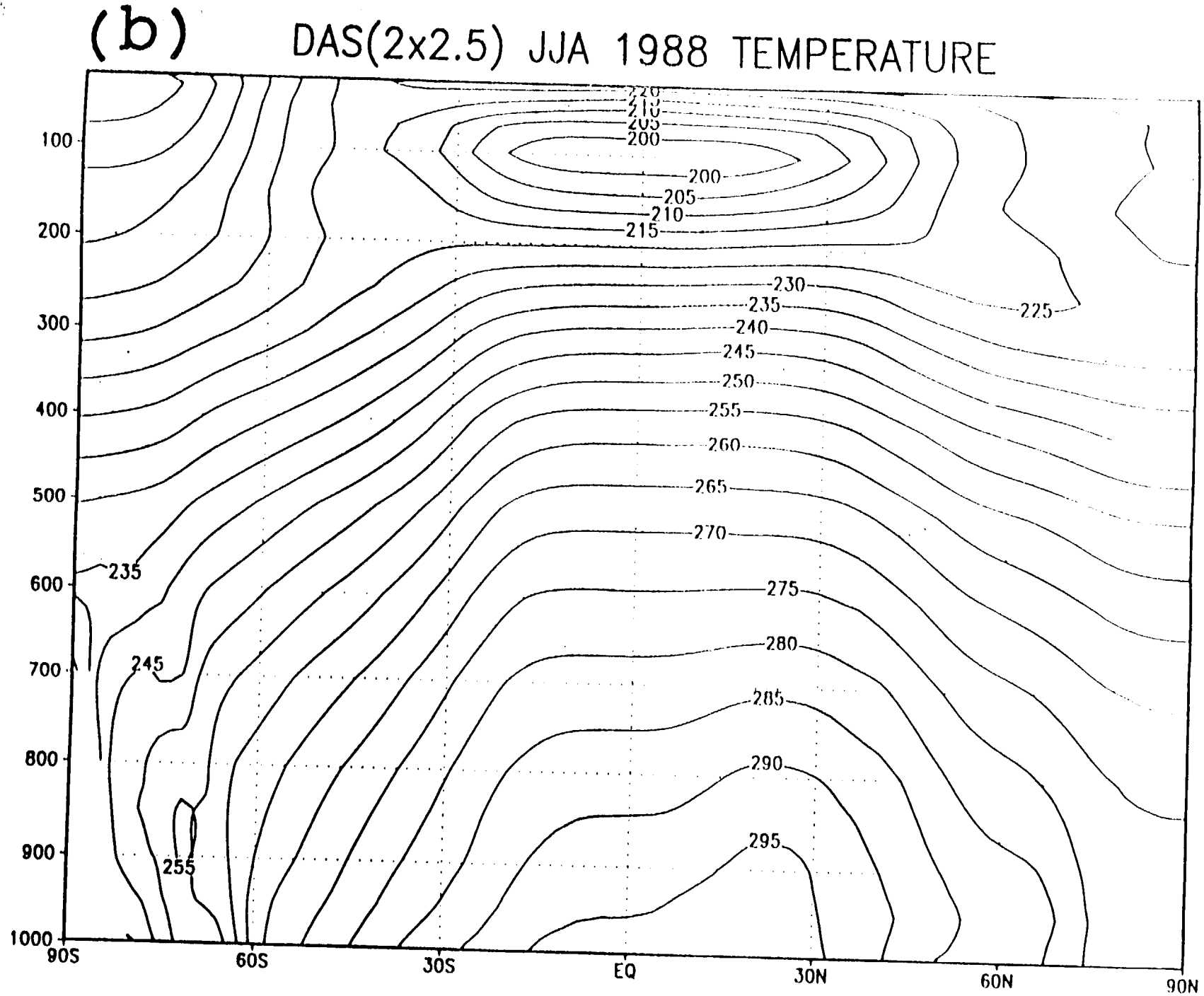

GrADS: COLA/IGES

1999 05 21 10:41

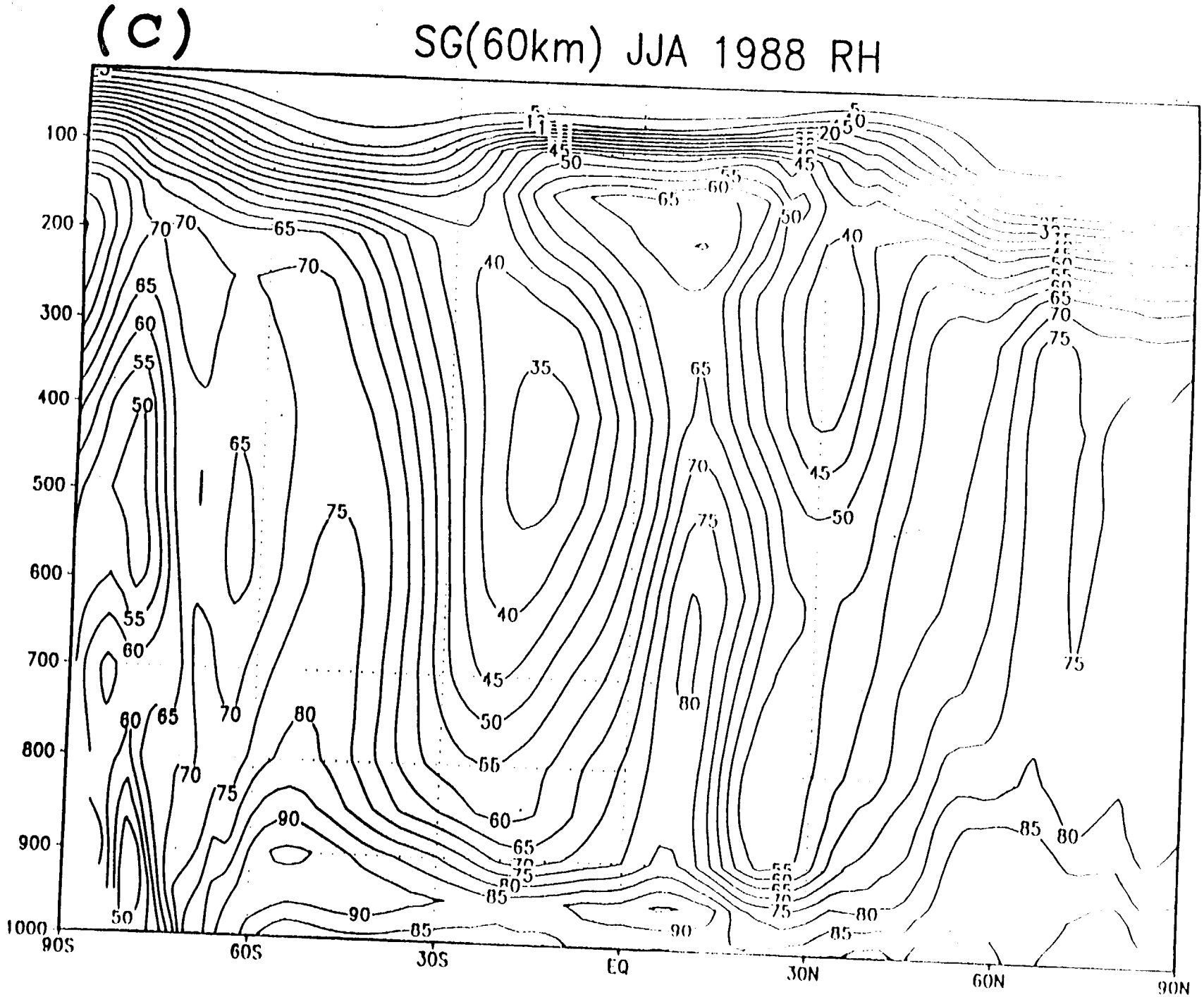

GrADS: COLA/IGES

1999 05 21 11:23

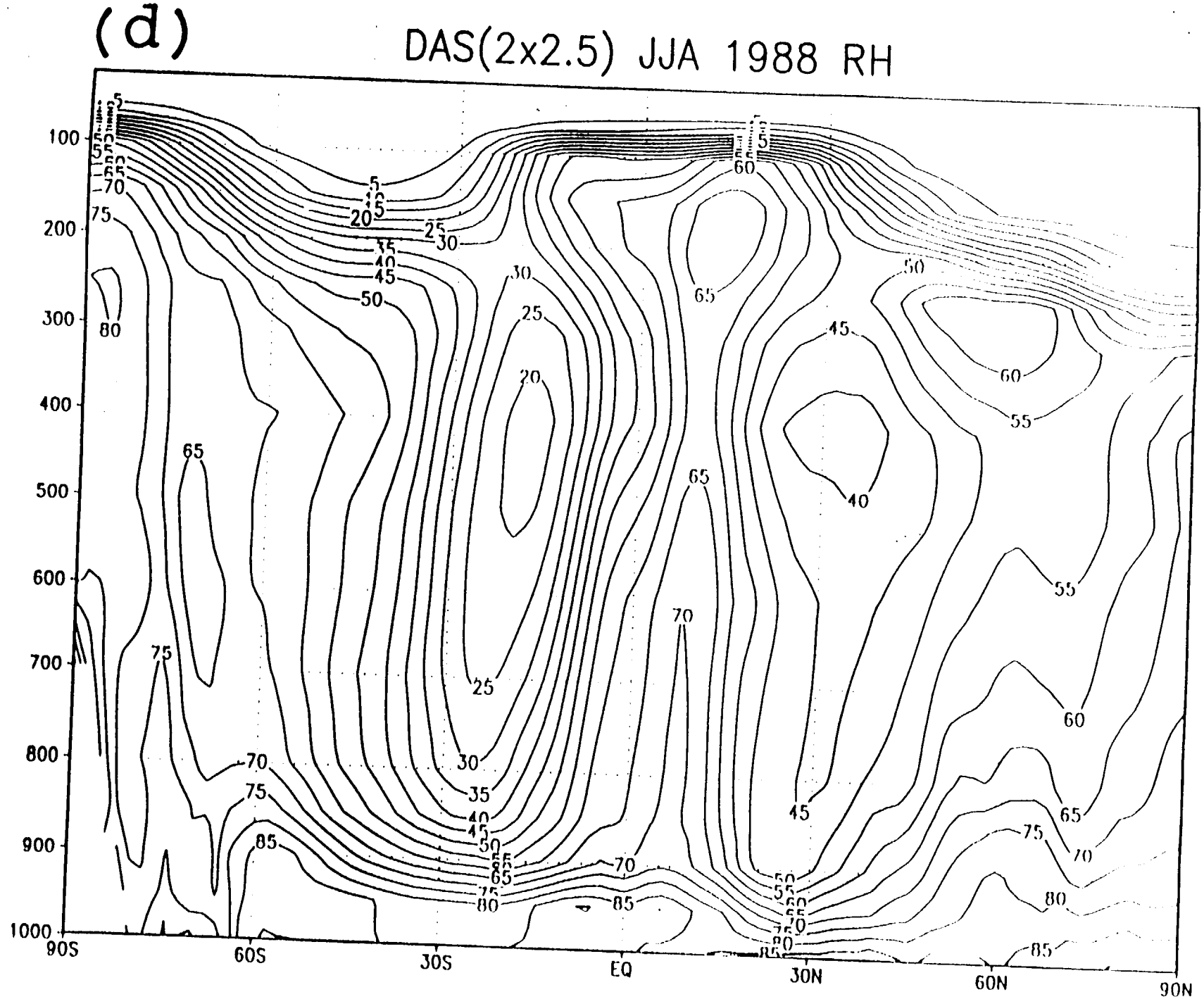

GrADS: COLA/IGES

1999 06 01 10:41

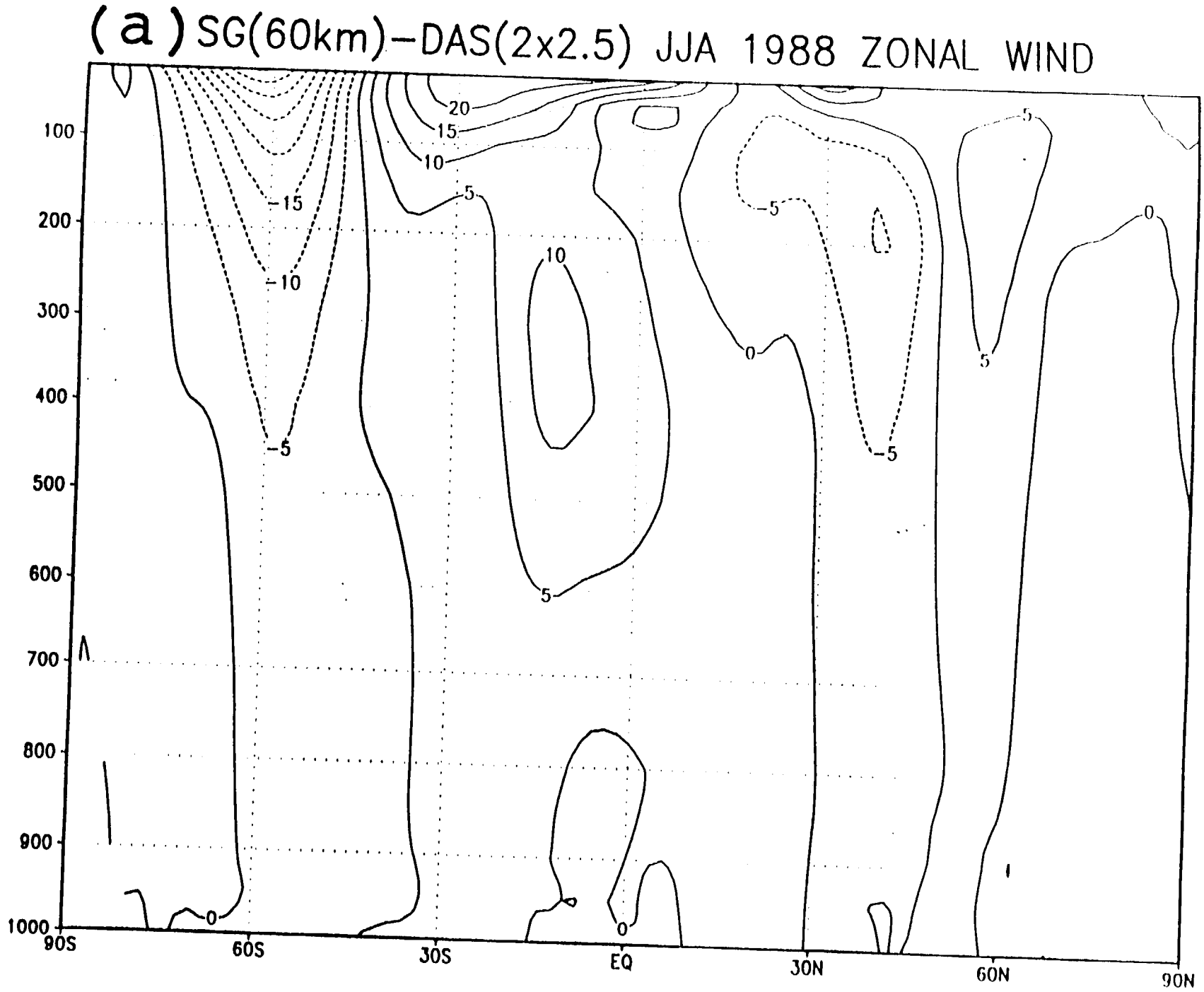

GrADS: COLA/IGES

1999-06-01-10:43

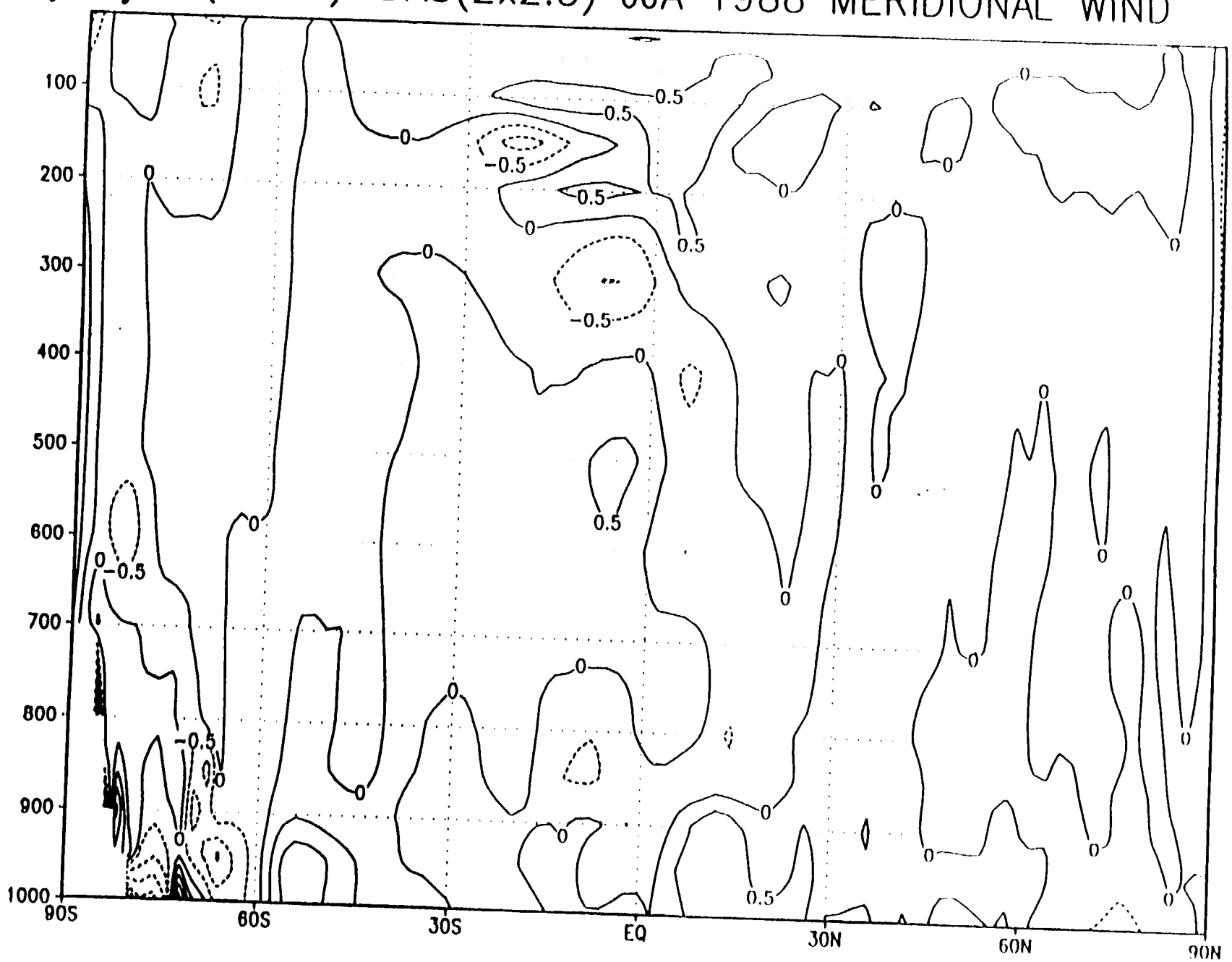

GrADS: COLA/IGES

1999-06-01-10:45

(C) SG(60km)-DAS(2x2.5) JJA 1988 TEMPERATURE

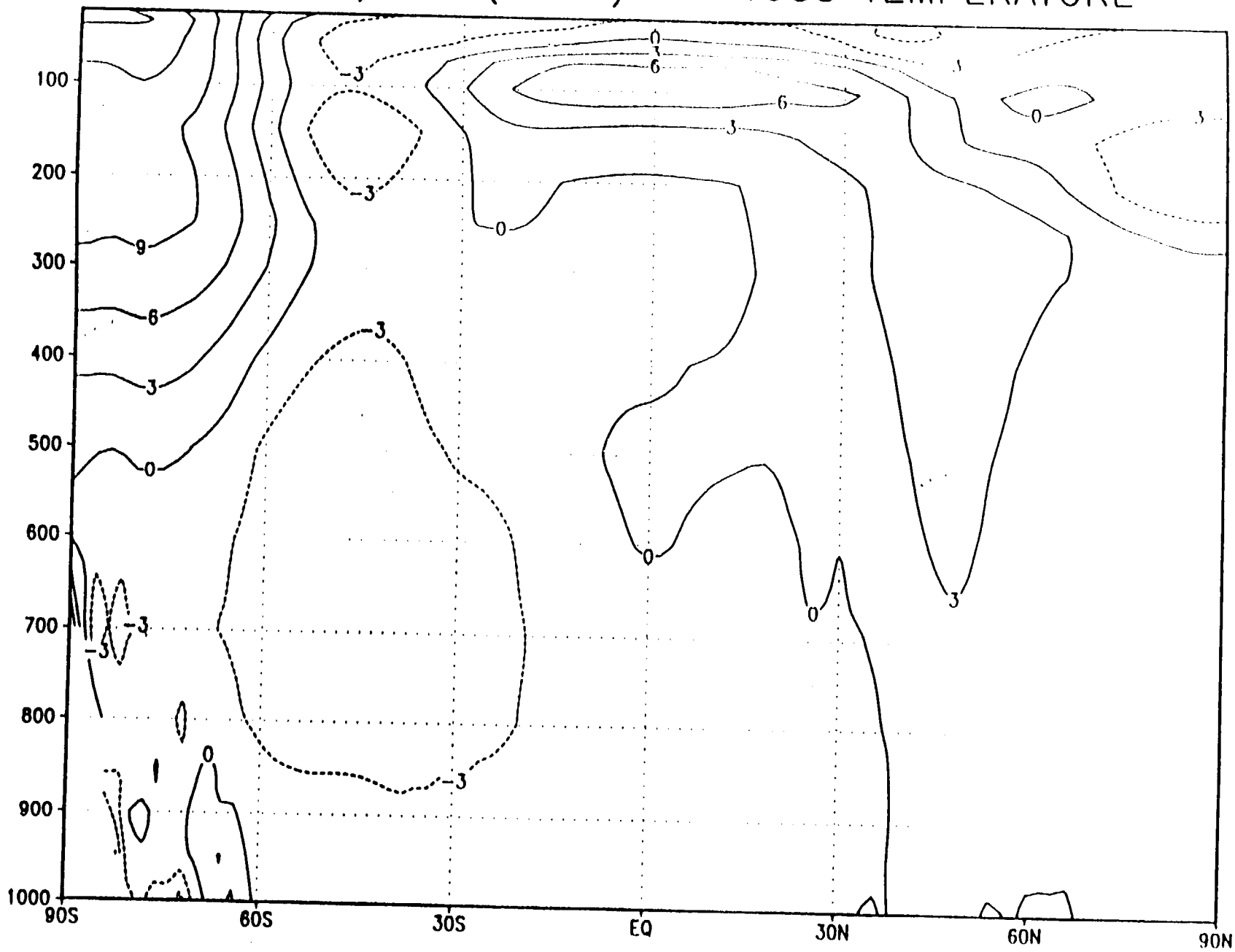

GrADS: COLA/IGES

1999-06-01-10:47

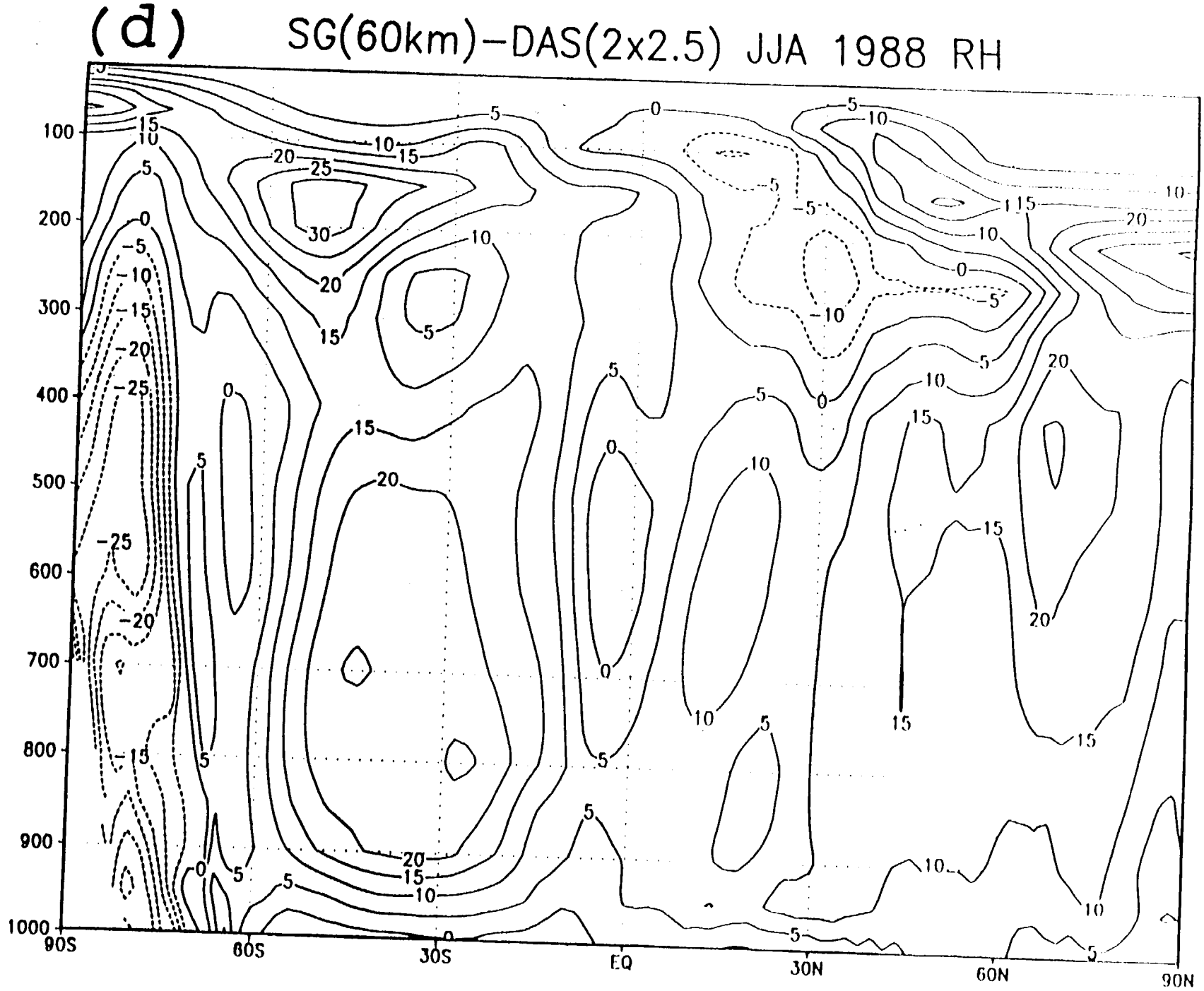

GrADS: COLA/IGES

1999 06 01 10:42

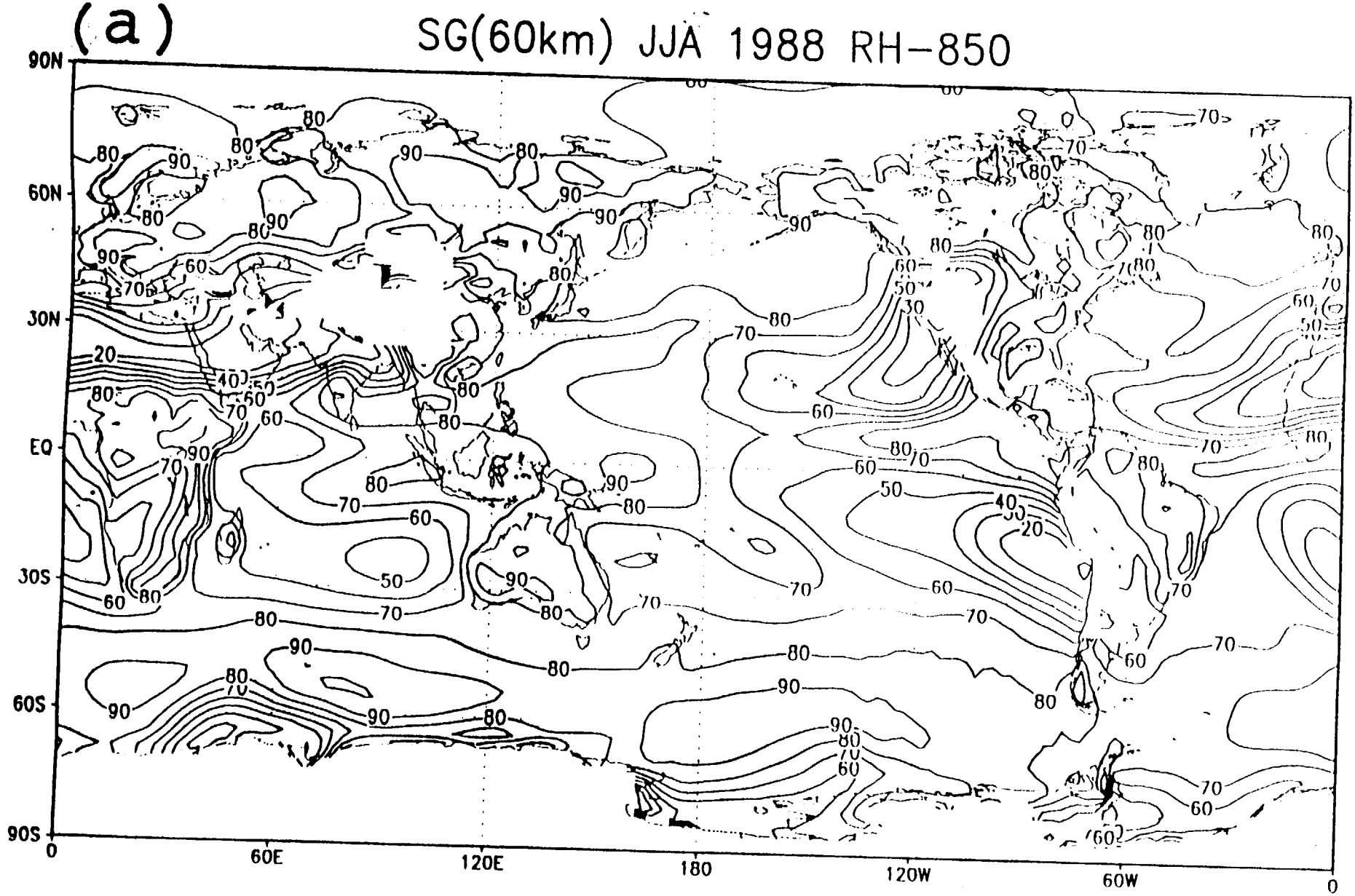

GrADS: COLA/IGES

1999 05 21 11:15

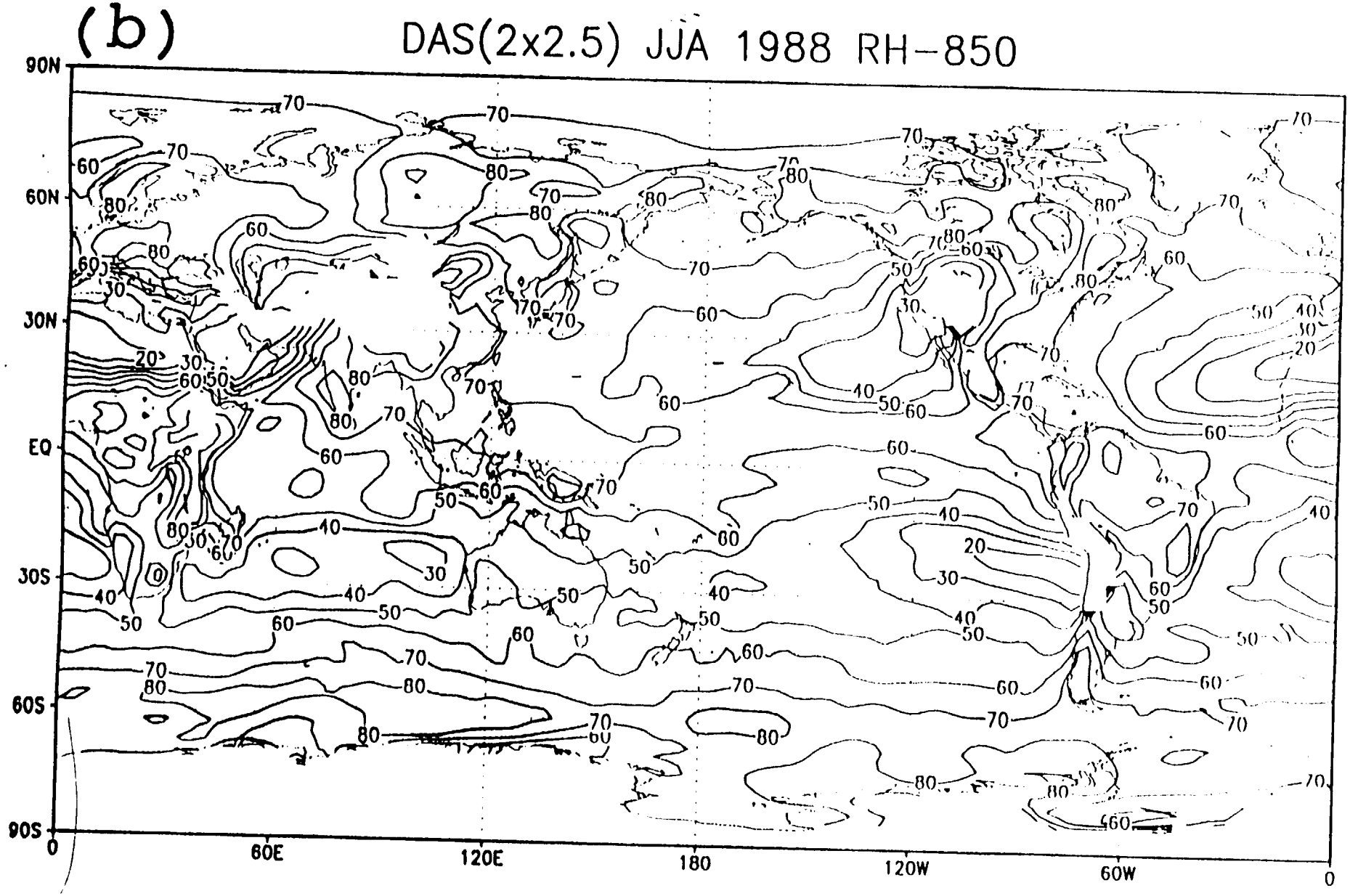

GrADS: COLA/IGES

1999-06-01-10:21

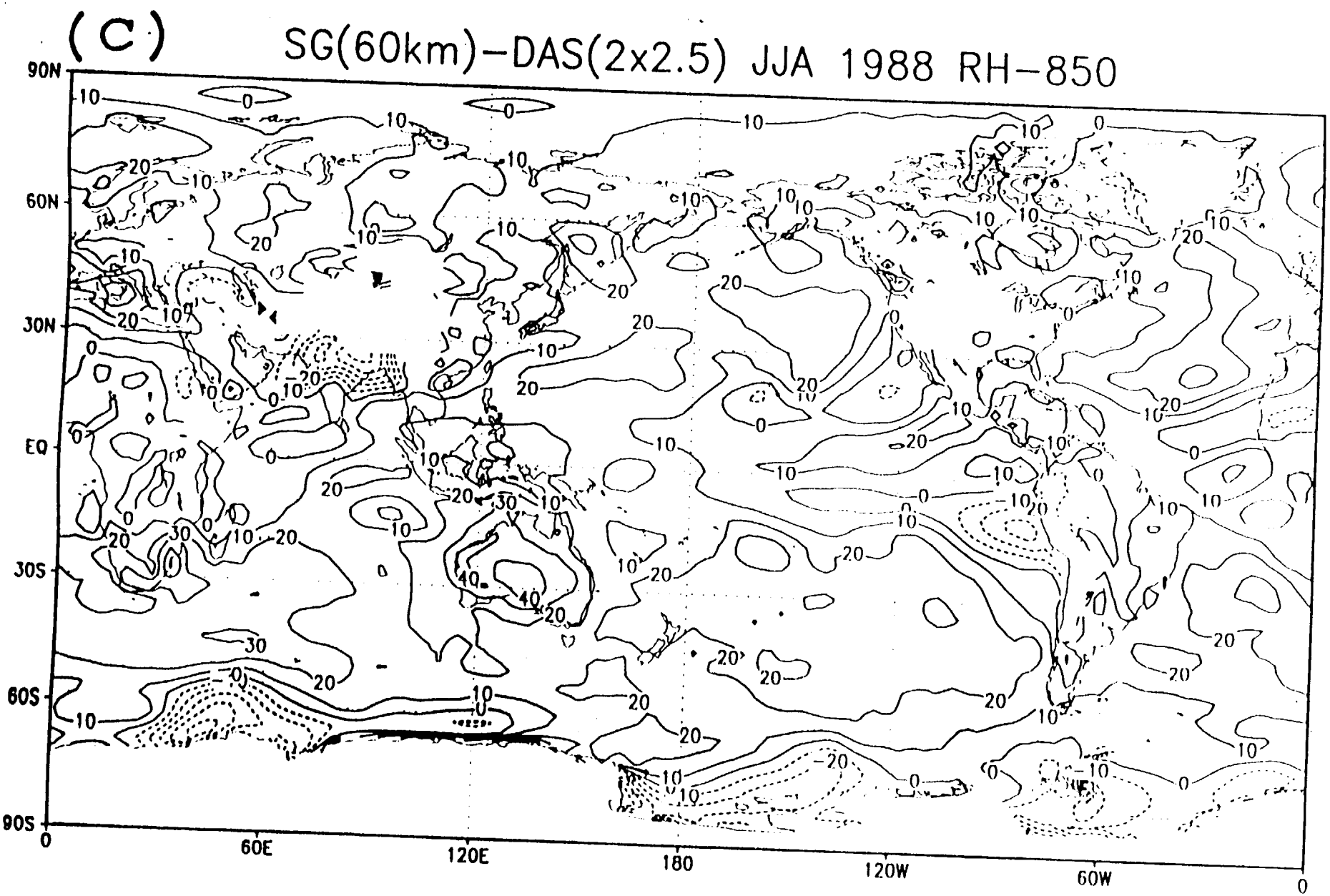

GrADS: COLA/IGES

1999-06-01-10:22

a) Rainfall Anomaly – June 1988

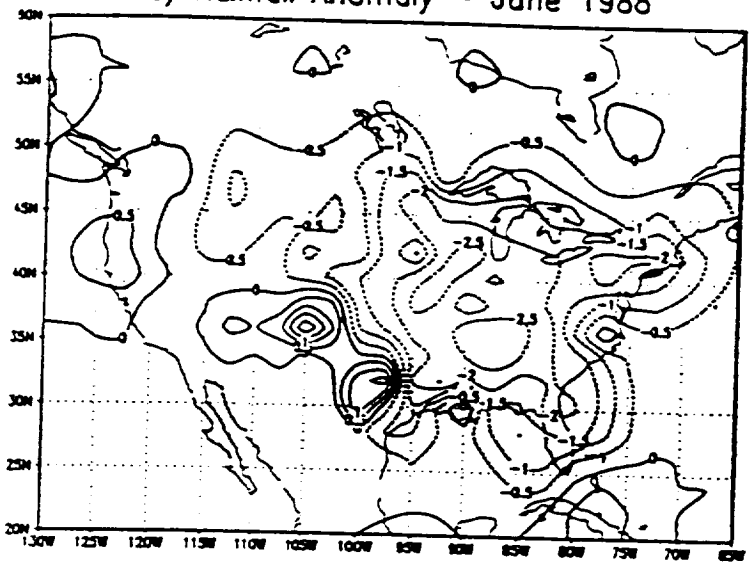

b) 500 mb Geop. Anomaly – June 1988

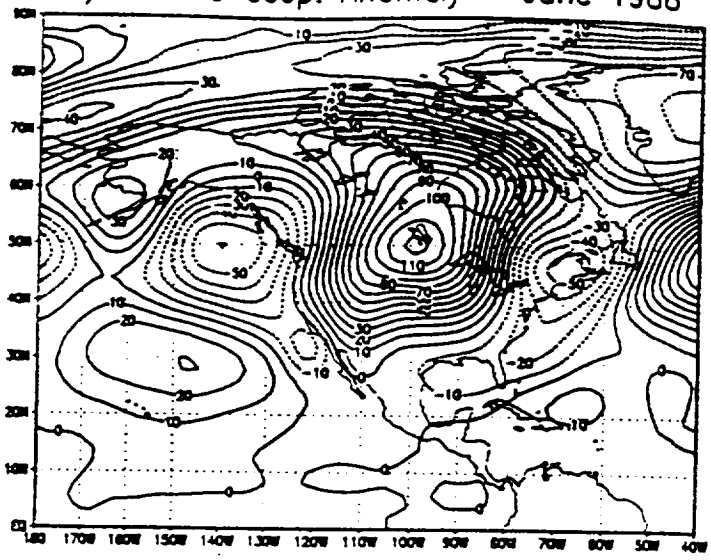

(c) JUNE 1988 NCEP PRECIPITATION

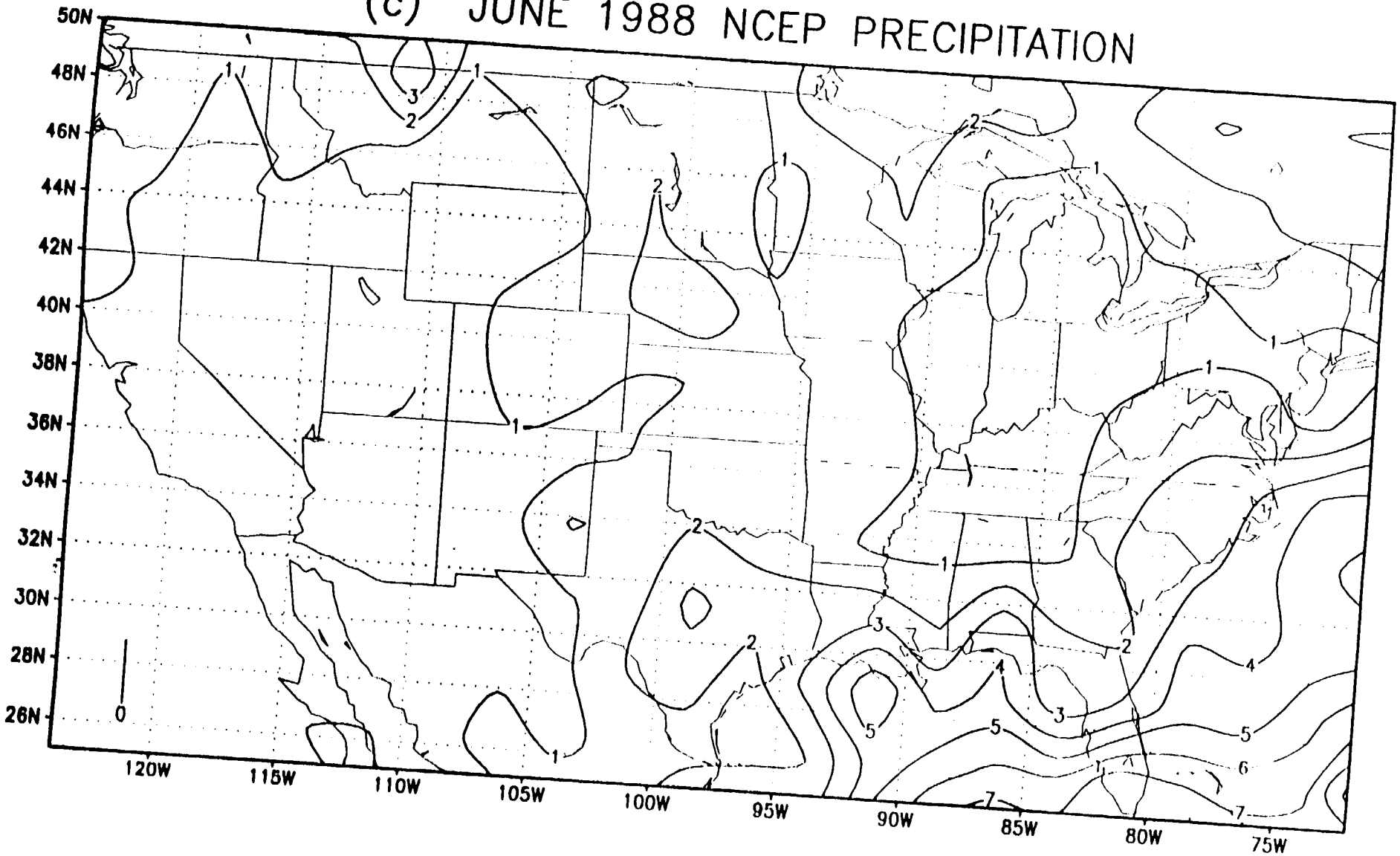

GrADS: COLA/IGES

2000-03-06-17:30

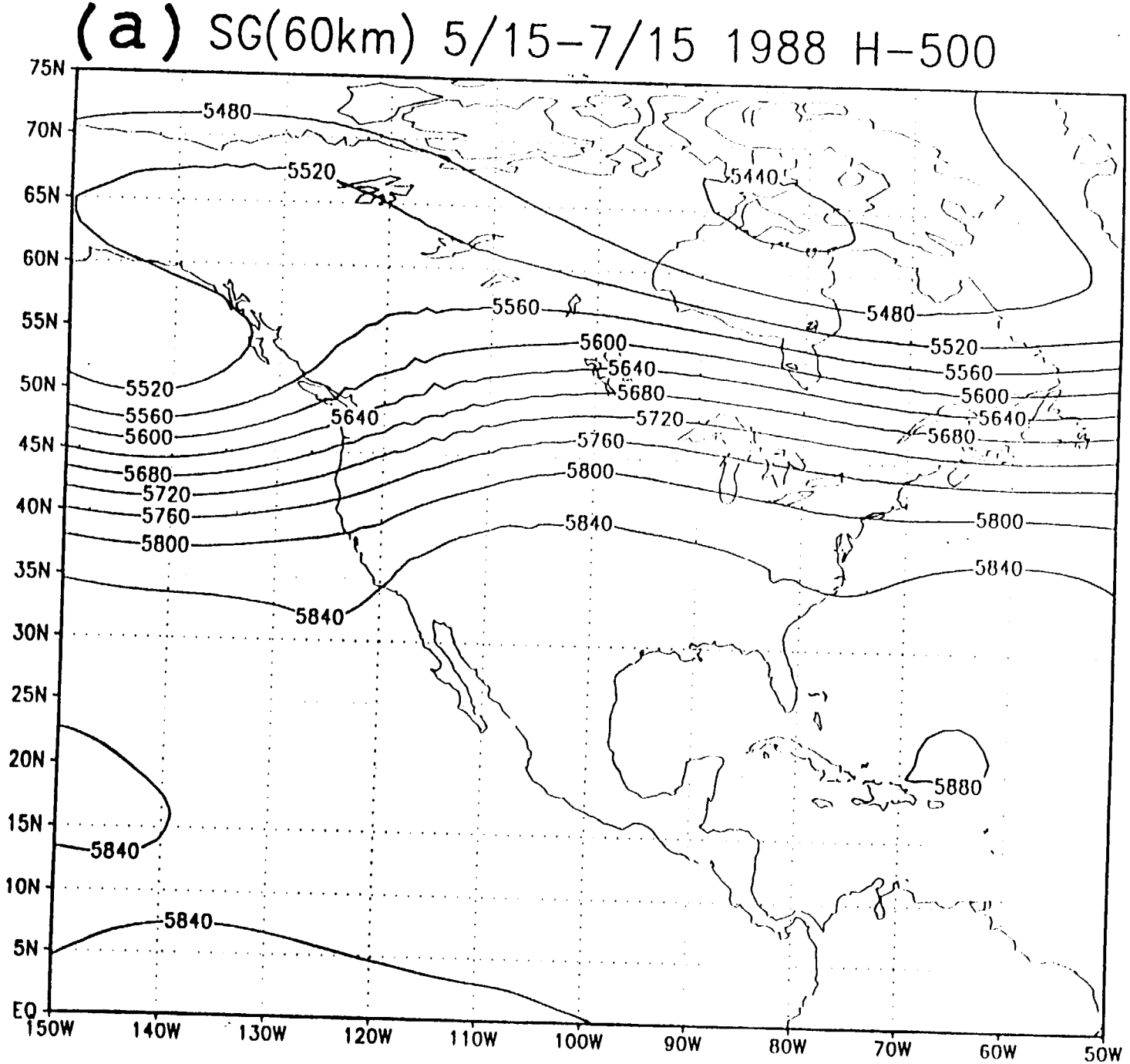
(a) SG(60km) 5/15-7/15 1988 H-500
75N
70N
65N
60N
55N
50N
45N
40N
35N
30N
25N
20N
15N
10N
5N
EQ
150W
140W
130W
120W
110W
100W
90W
80W
70W
60W
50W
5480
5520
5560
5600
5640
5680
5720
5760
5800
5840
5880
GrADS: COLA/IGES
1999-10-28-18:18

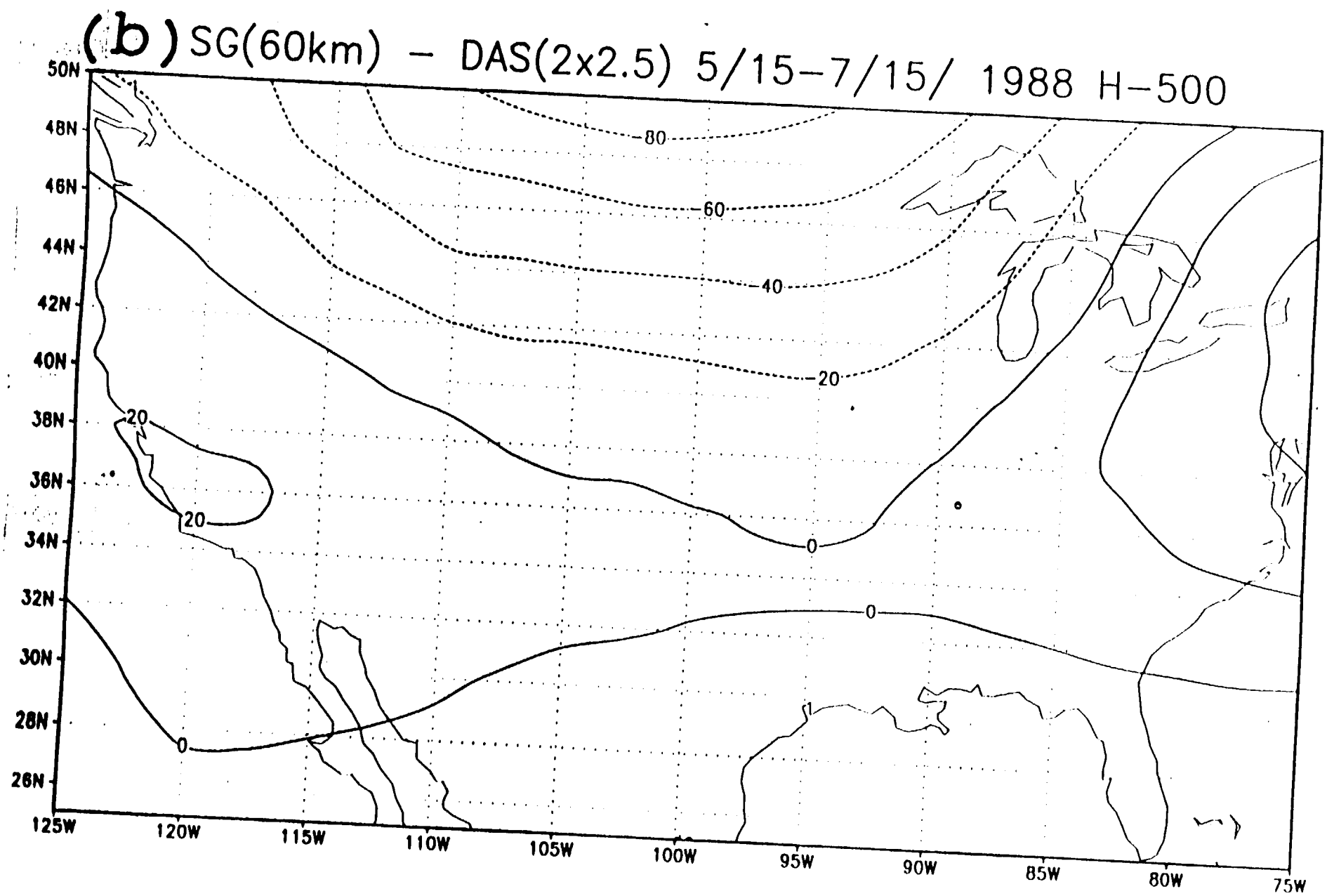

GrADS: COLA/IGES

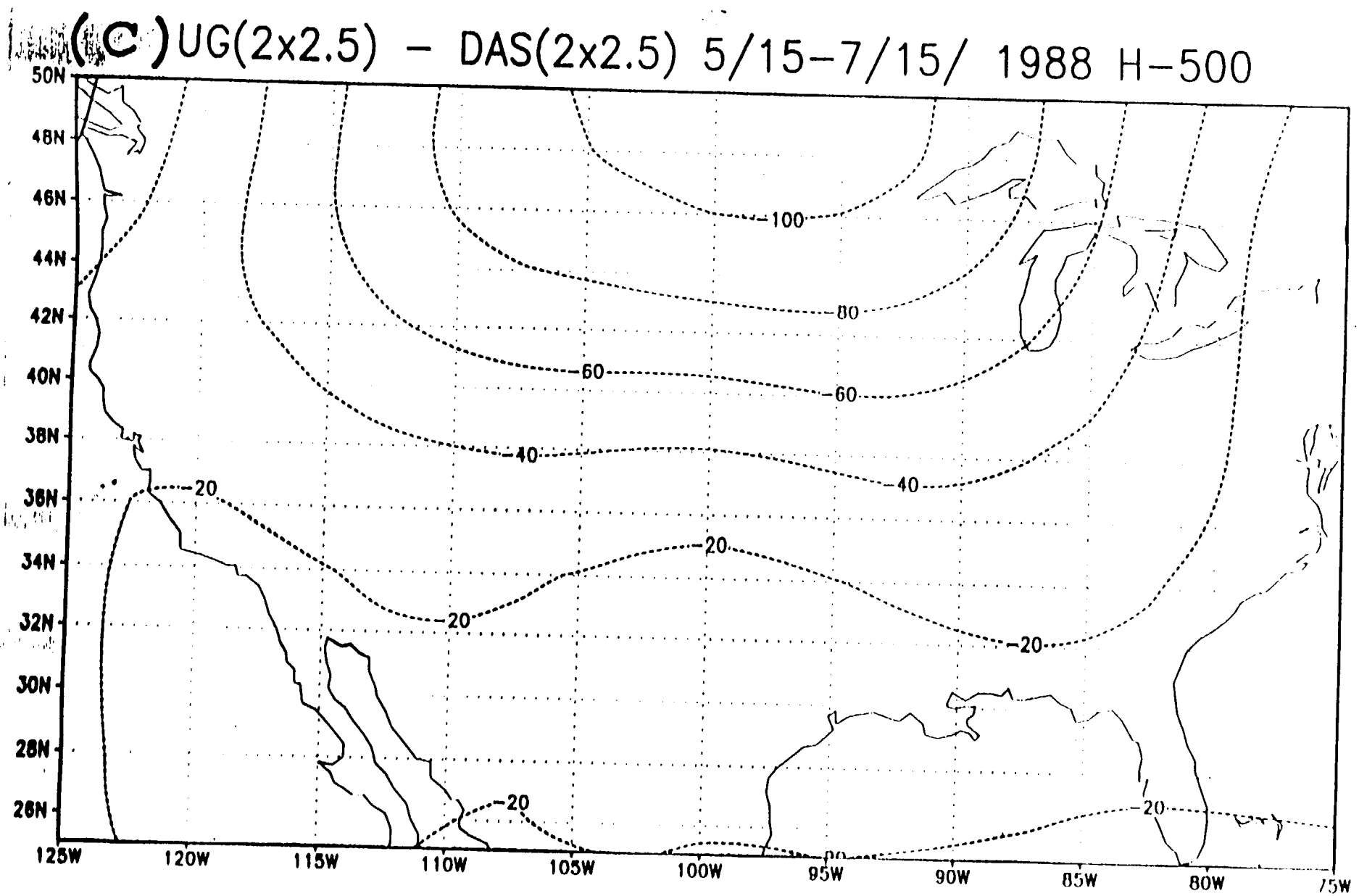

GrADS: COLA/IGES

1998-11-13-15:31

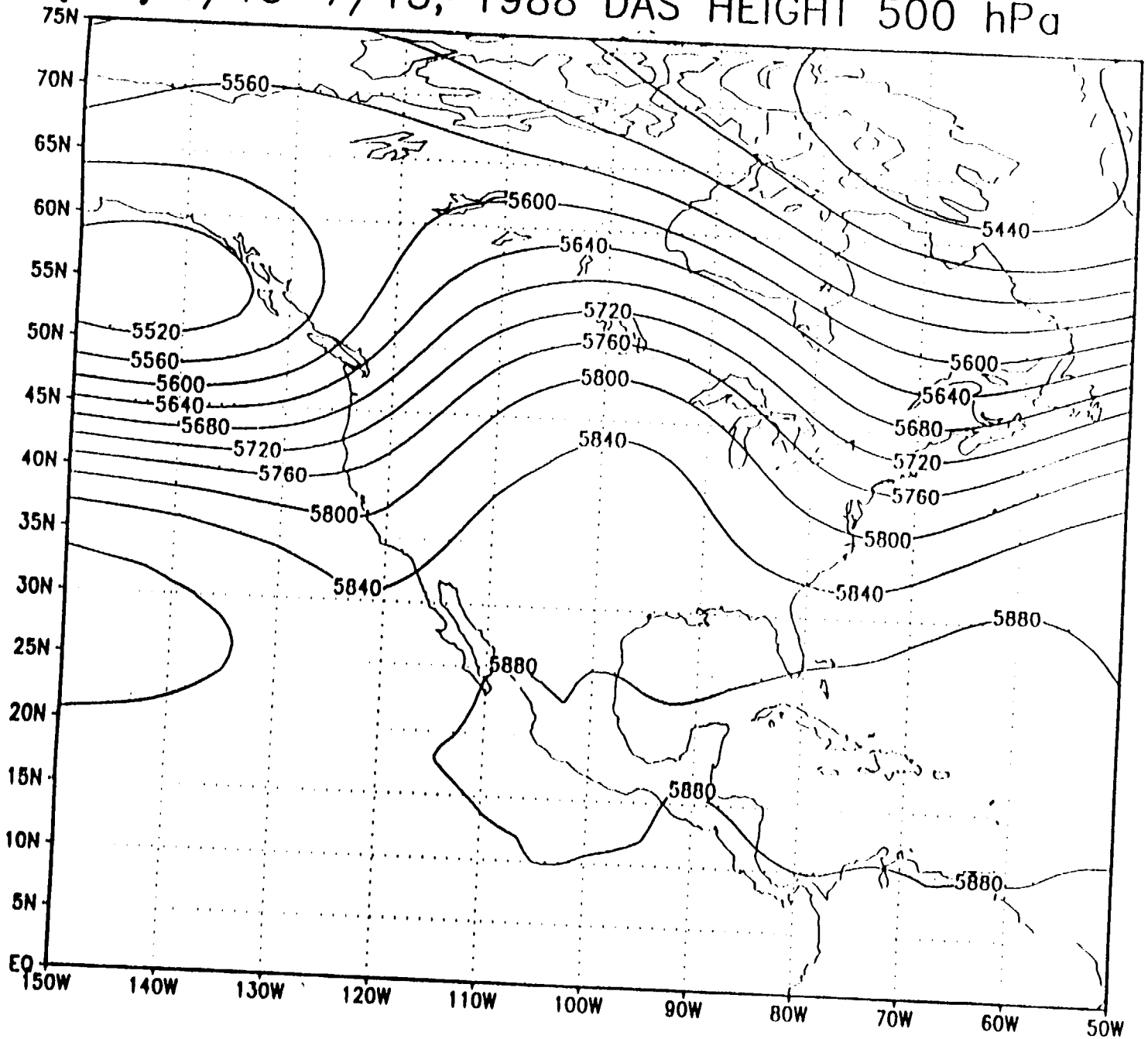

IS: COLA/IGES

1998 07 08 14:22

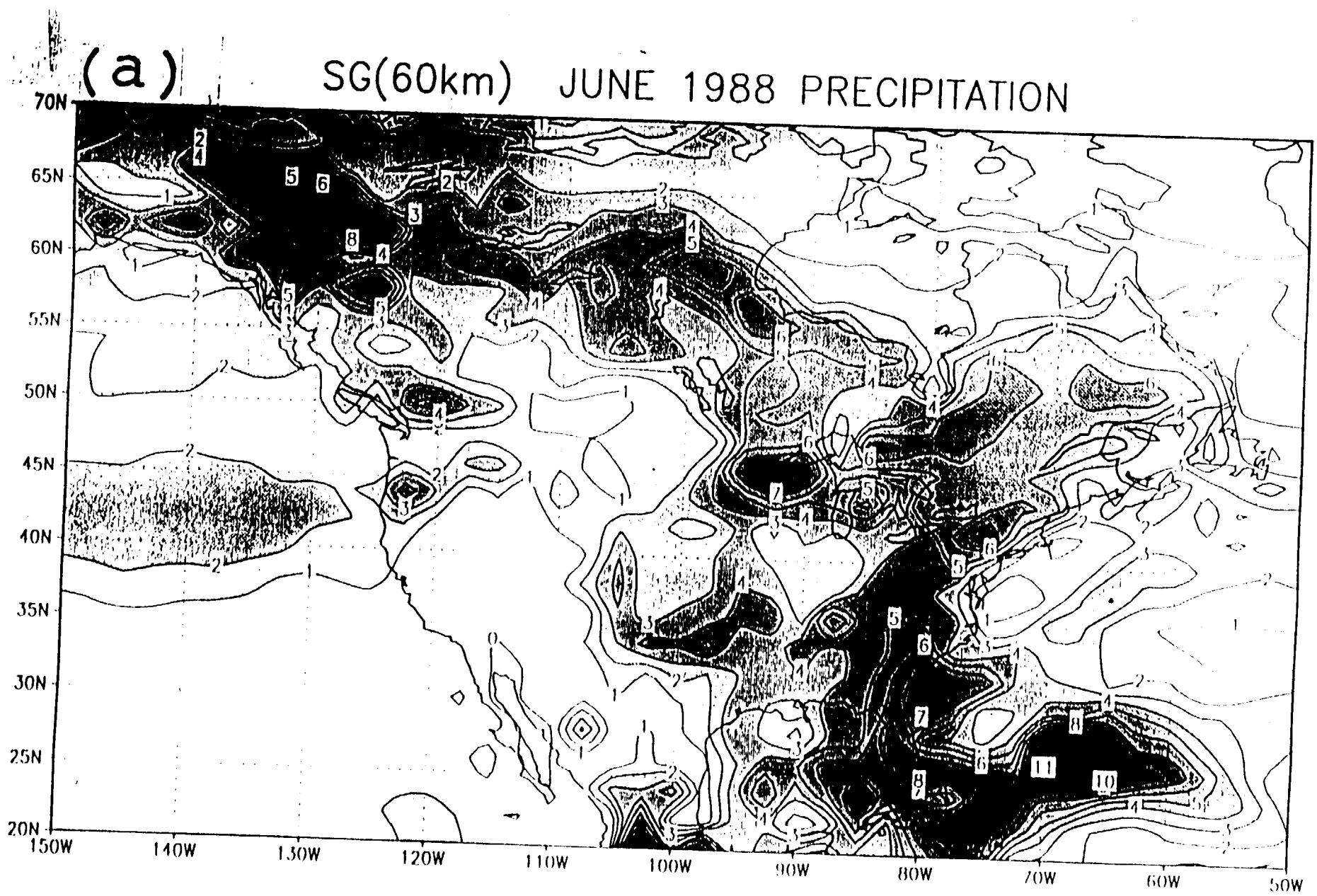

GrADS: COLA/IGES

1998-11-13-11:10

(b) SG(60km) – DAS(2x2.5) JUNE 1988 PRECIPITATION

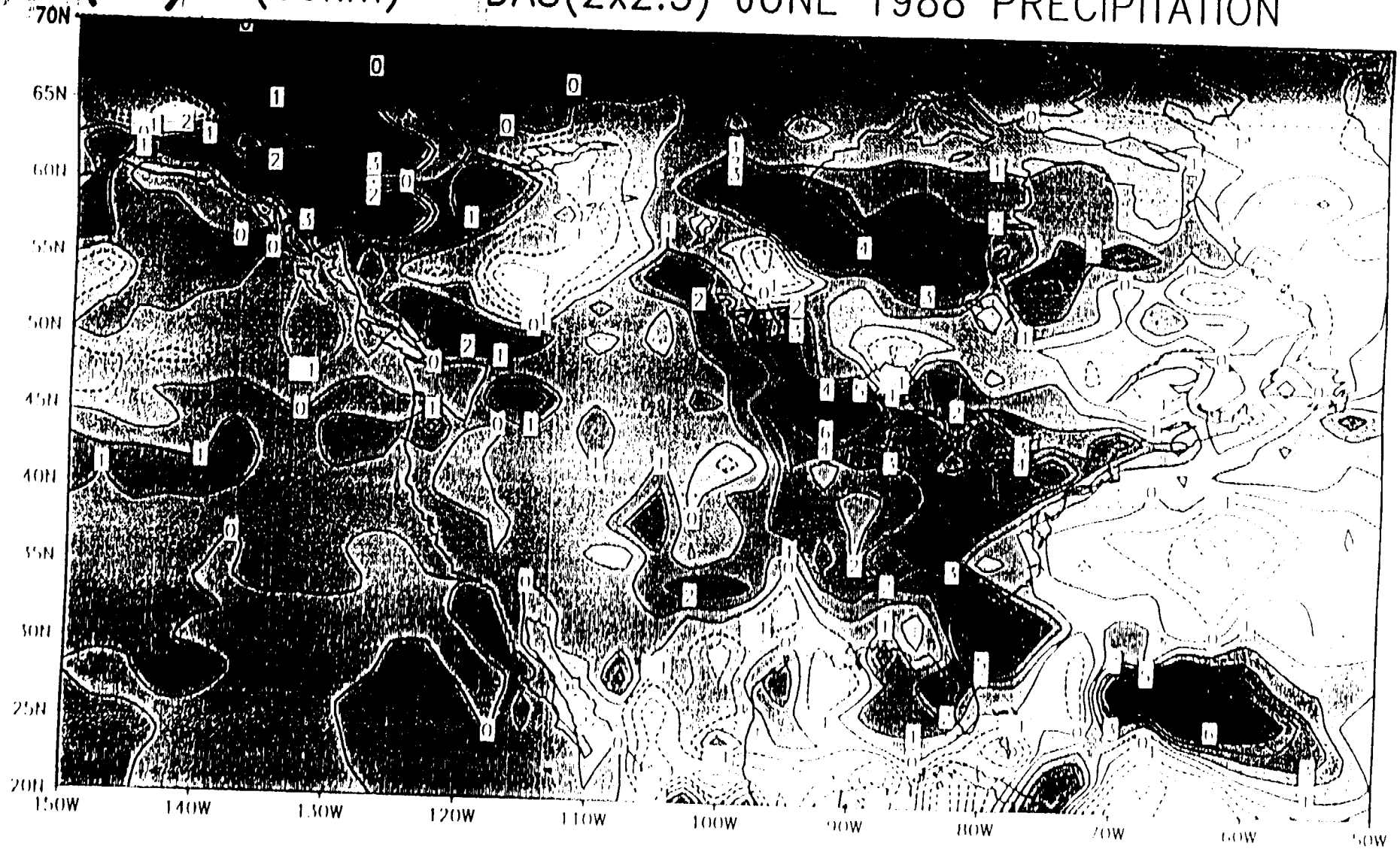

GrADS: COLA/IGES

1998 11-13-11:36

(C) UG(2x2.5) – DAS(2x2.5) JUNE 1988 PRECIPITATION

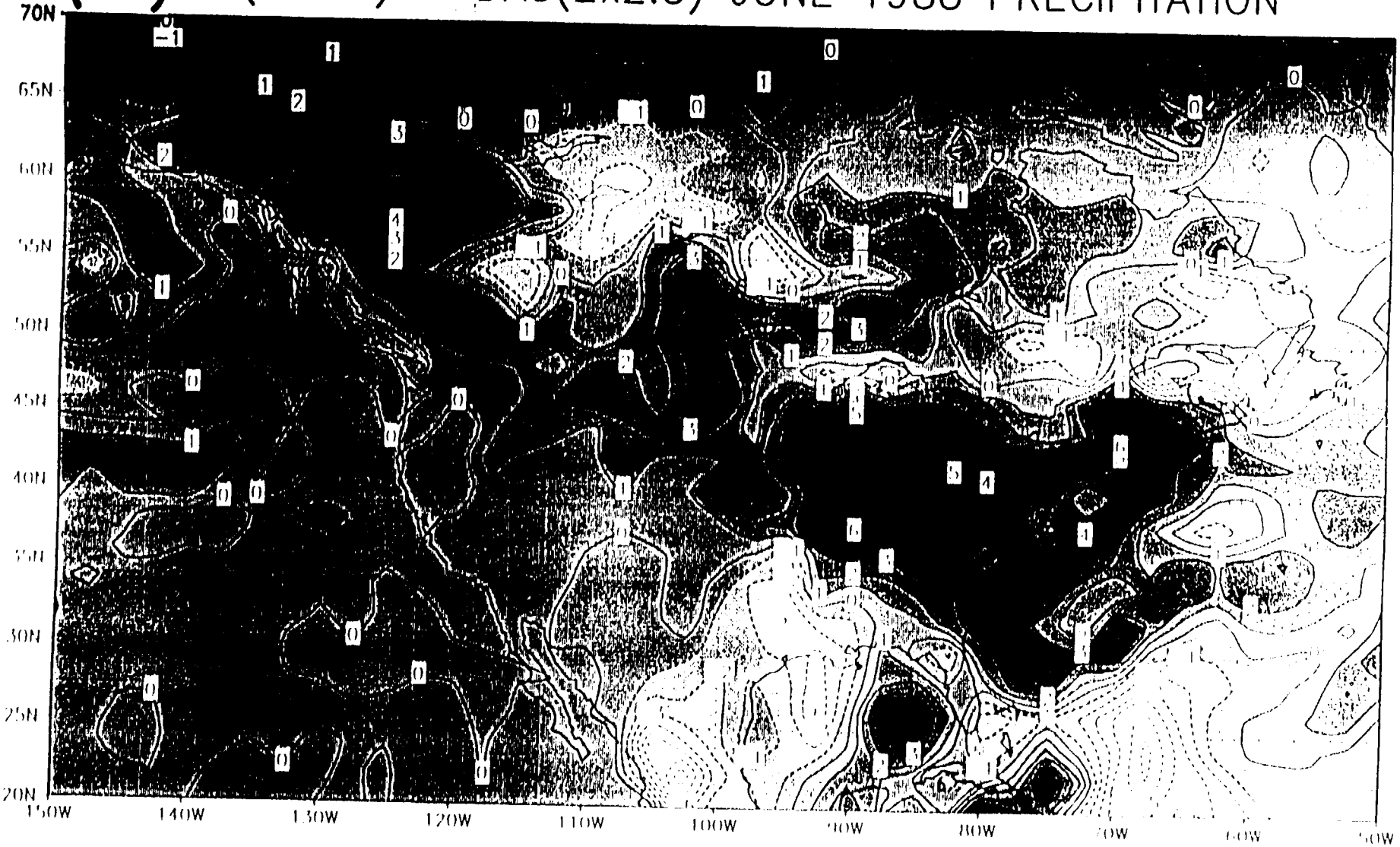

GrADS: COLA/IGES

1998-11-13-11:35

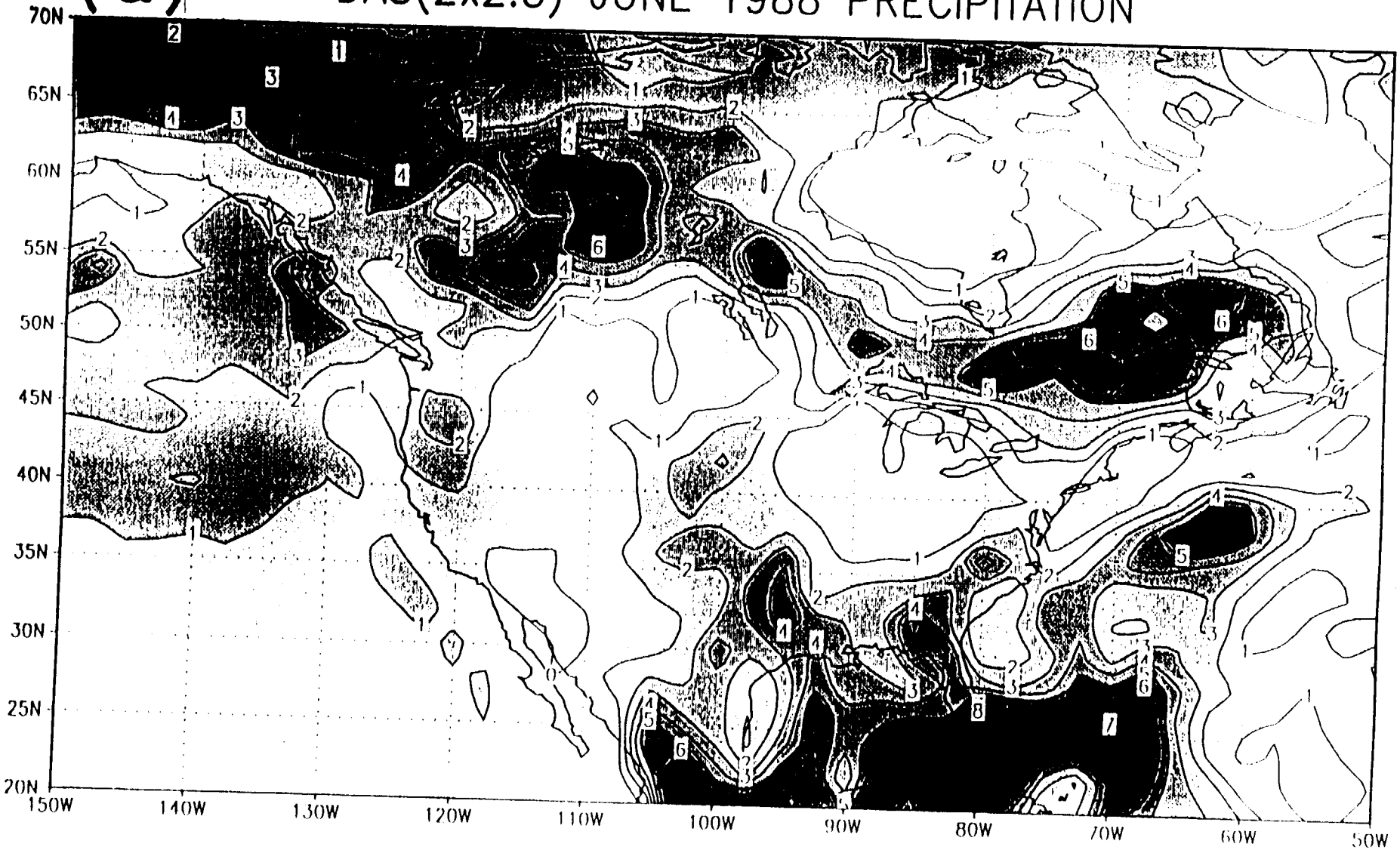

GrADS: COLA/IGES

1998-11-13-11:07

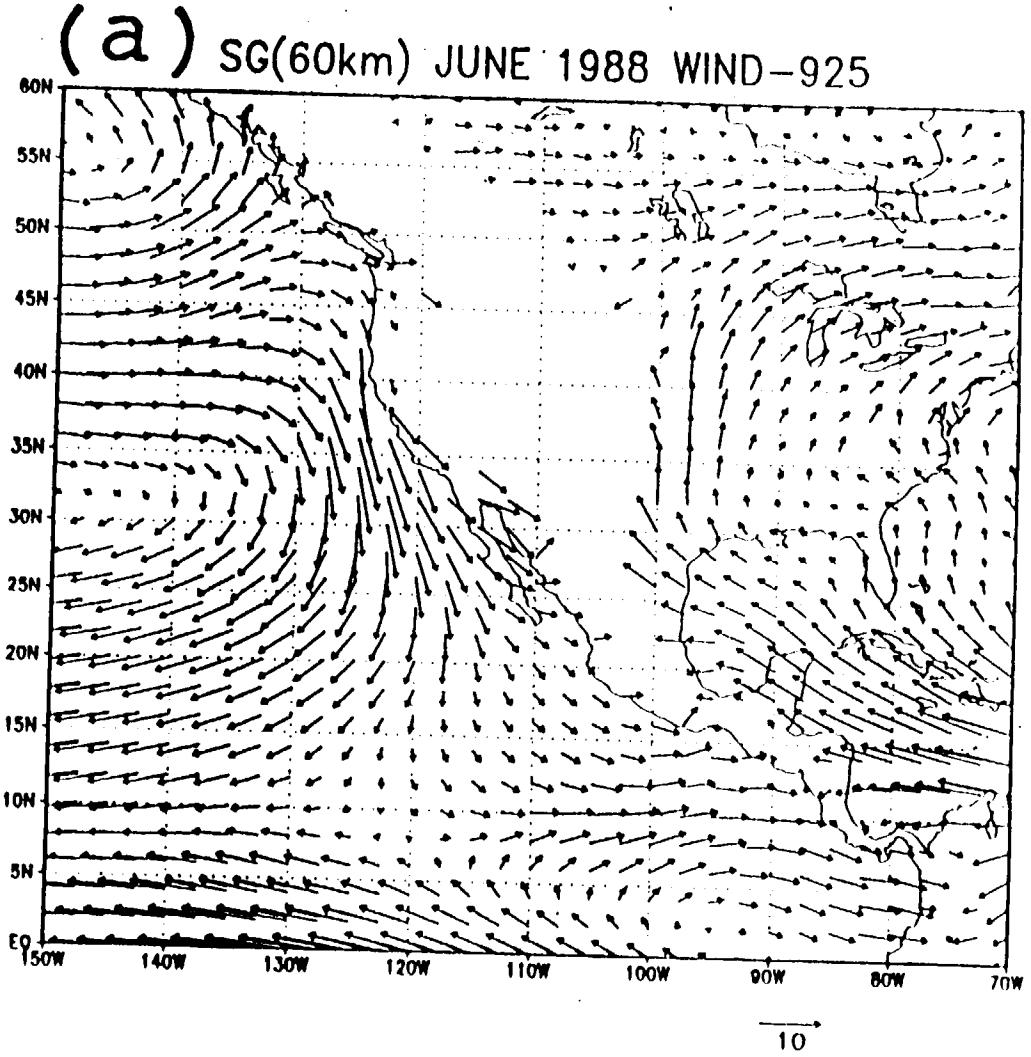
(a) SG(60km) JUNE 1988 WIND-925
60N
55N
50N
45N
40N
35N
30N
25N
20N
15N
10N
5N
EQ
150W
140W
130W
120W
110W
100W
90W
80W
70W
10
GrADS: COLA/IGES
1998-11-16-17:43

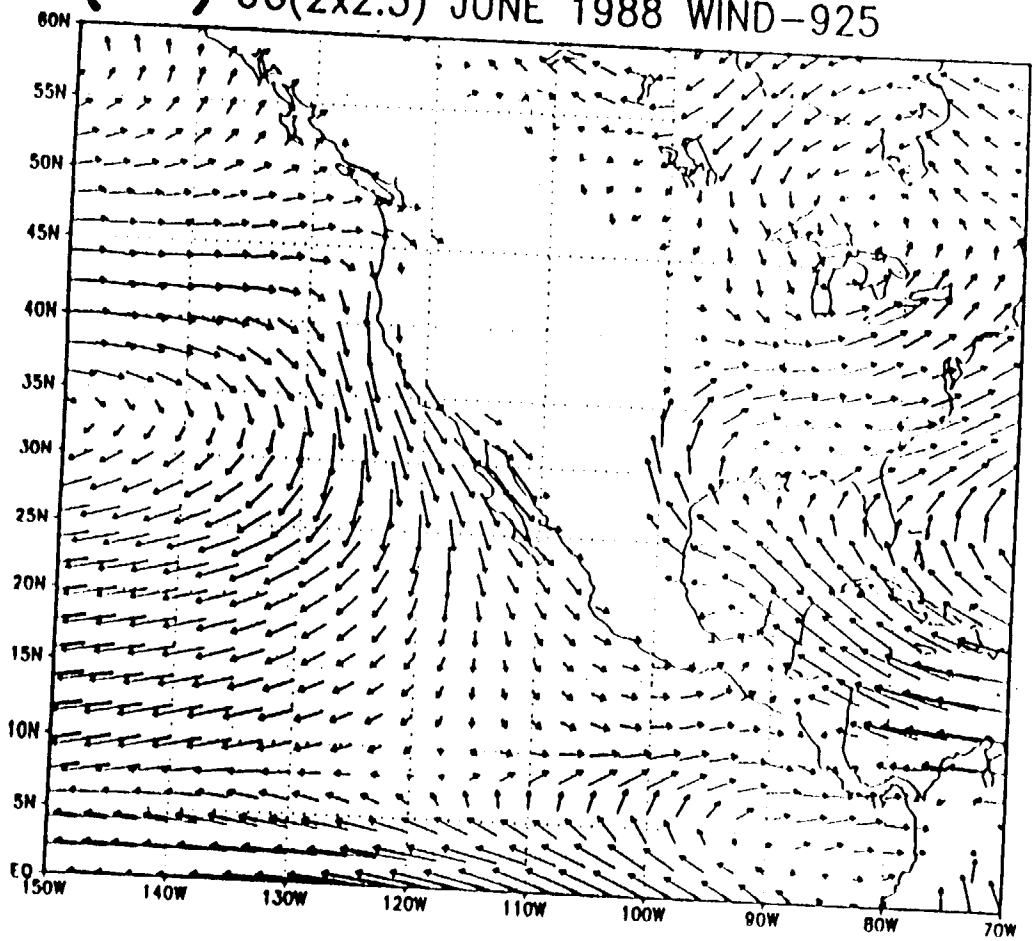

1998-11-18-10:21

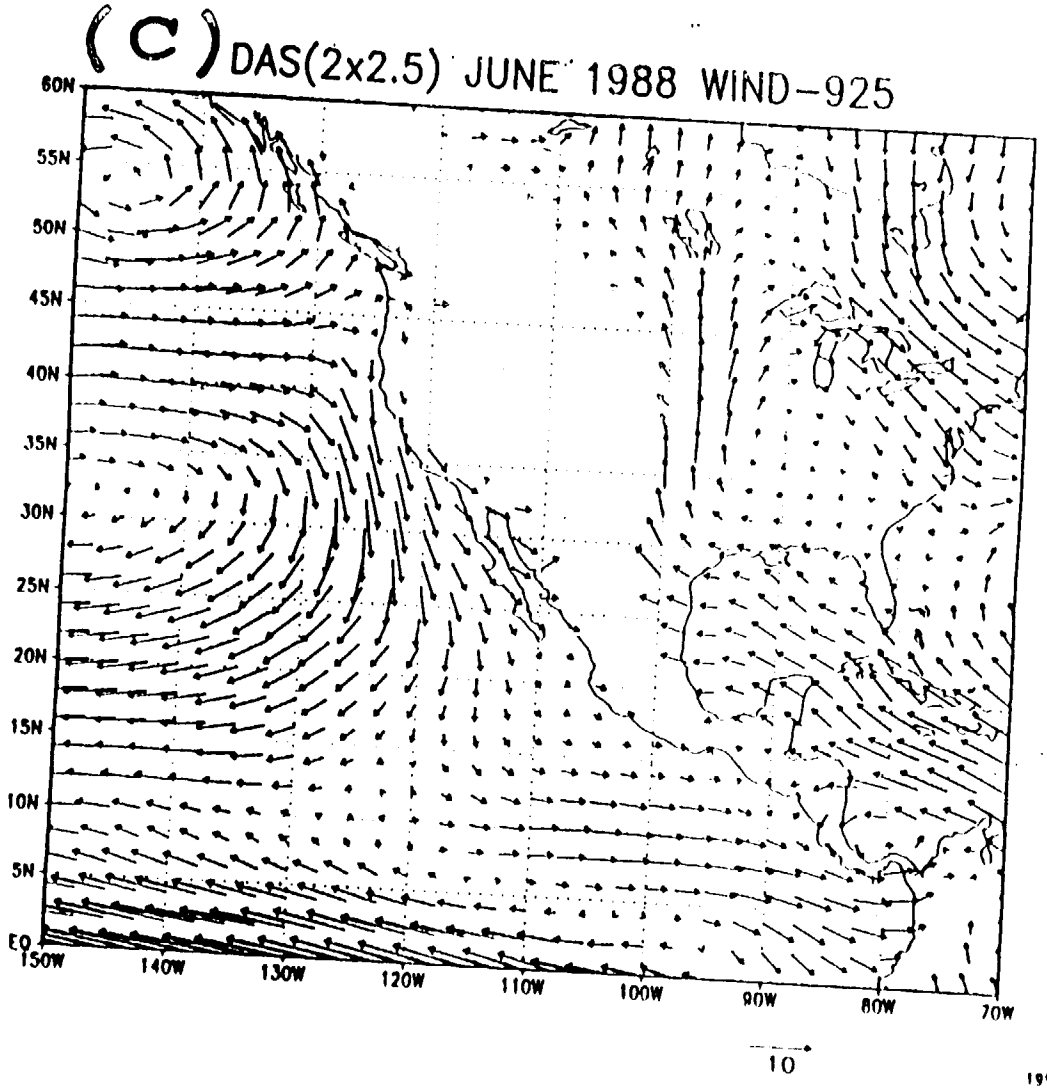
(c) DAS(2x2.5) JUNE 1988 WIND-925
60N
55N
50N
45N
40N
35N
30N
25N
20N
15N
10N
5N
EQ
150W
140W
130W
120W
110W
100W
90W
80W
70W
10
GrADS: COLA/IGES
1998-11-18-10:22

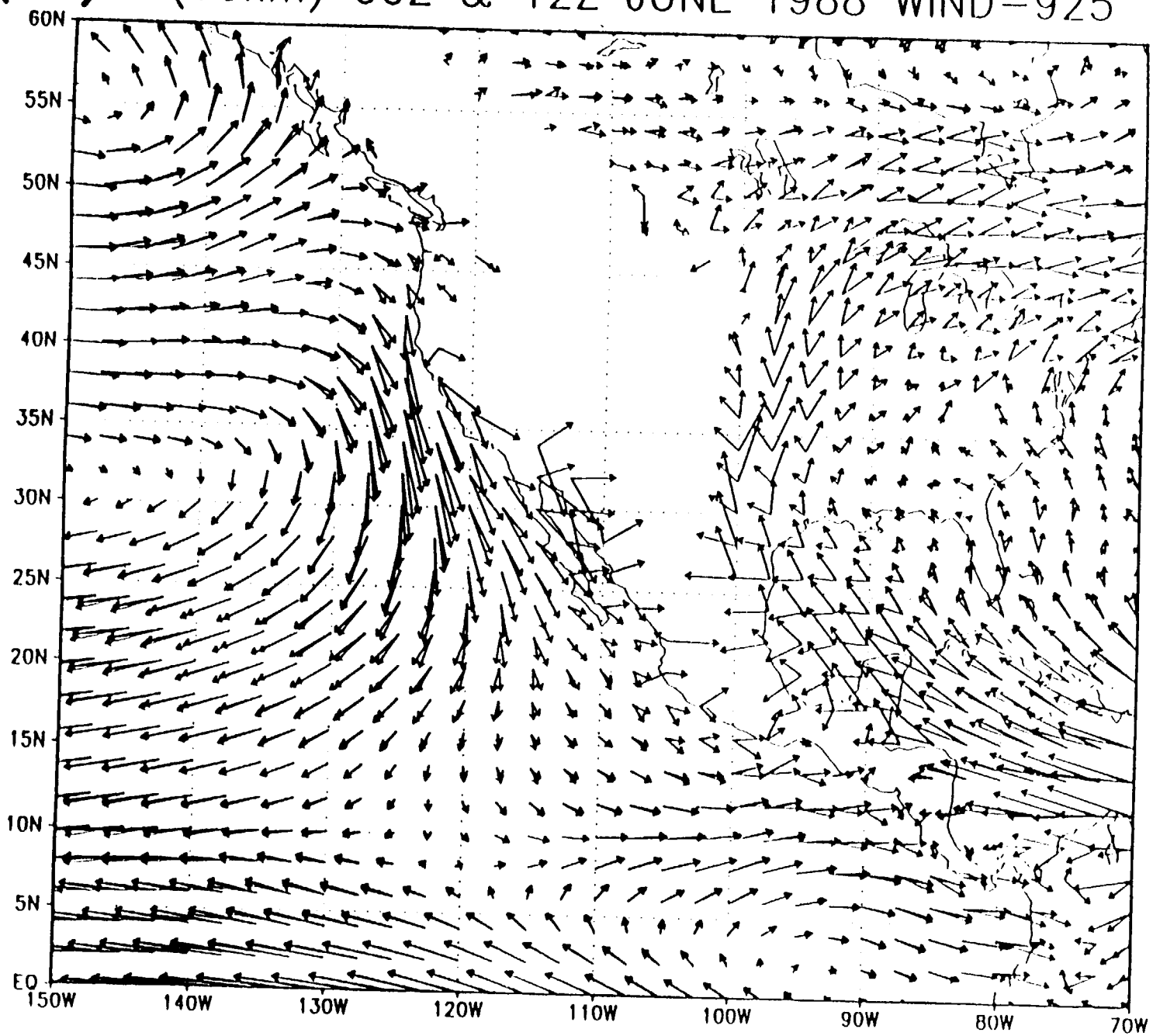
(a) SG(60km) 00Z & 12Z JUNE 1988 WIND-925
60N
55N
50N
45N
40N
35N
30N
25N
20N
15N
10N
5N
EQ
150W
140W
130W
120W
110W
100W
90W
80W
70W
10
GrADS: COLA/IGES
1998 11 17 11:55

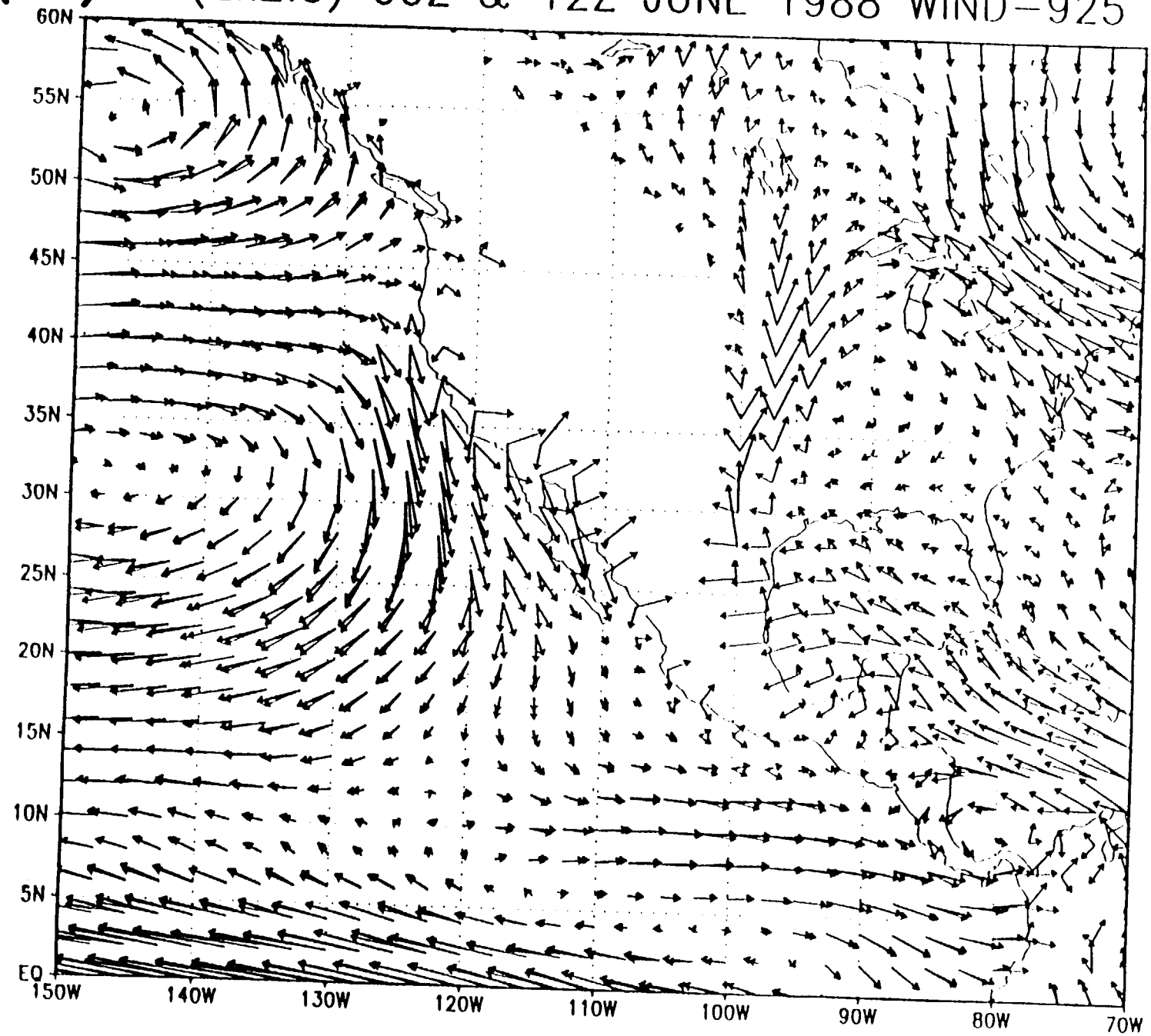
(b) DAS(2x2.5) 00Z & 12Z JUNE 1988 WIND-925
60N
55N
50N
45N
40N
35N
30N
25N
20N
15N
10N
5N
EQ
150W
140W
130W
120W
110W
100W
90W
80W
70W
GrADS: COLA/IGES
10
1998 11 17 12:00

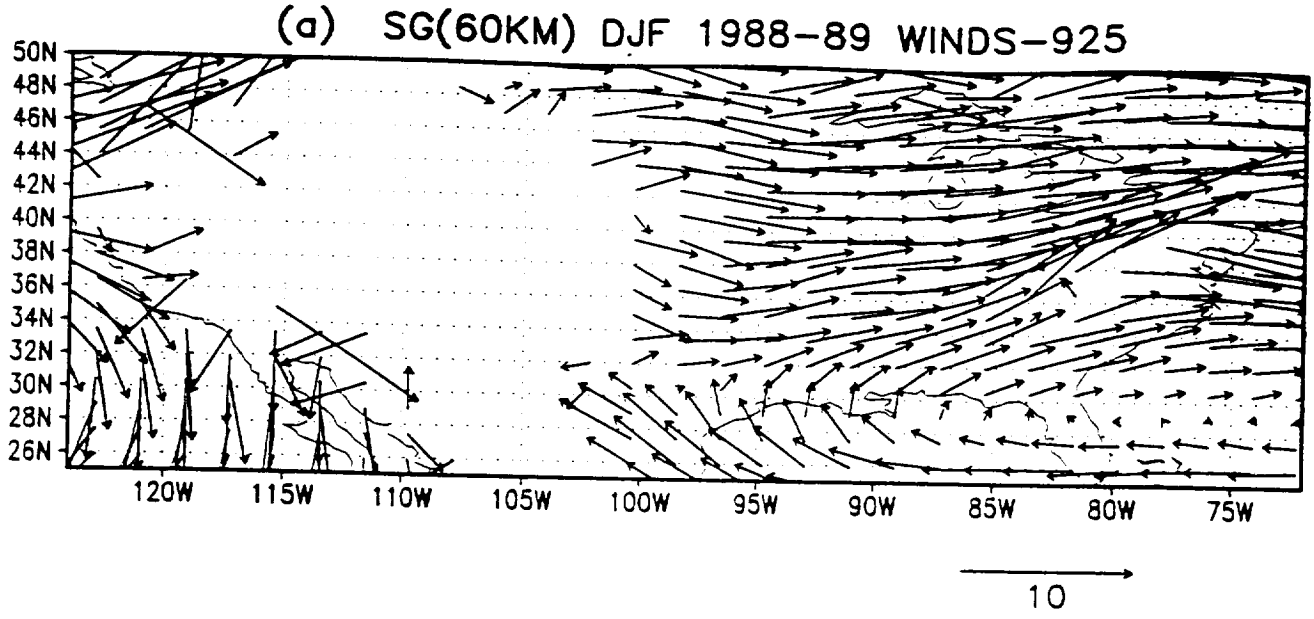

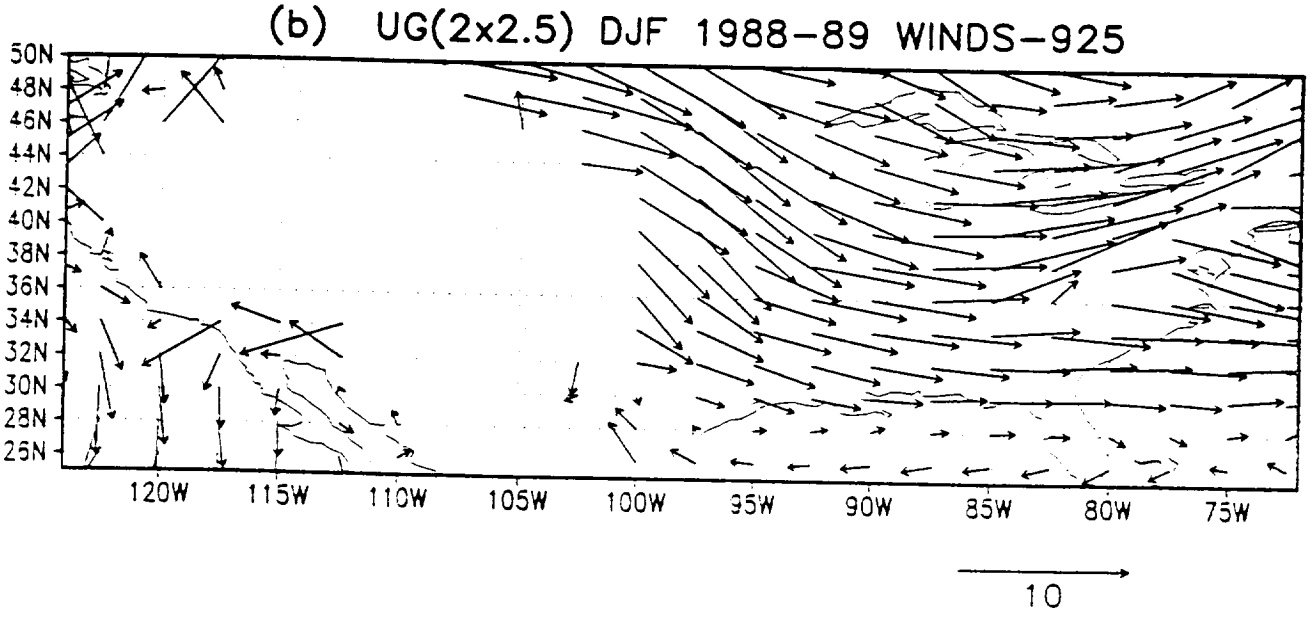

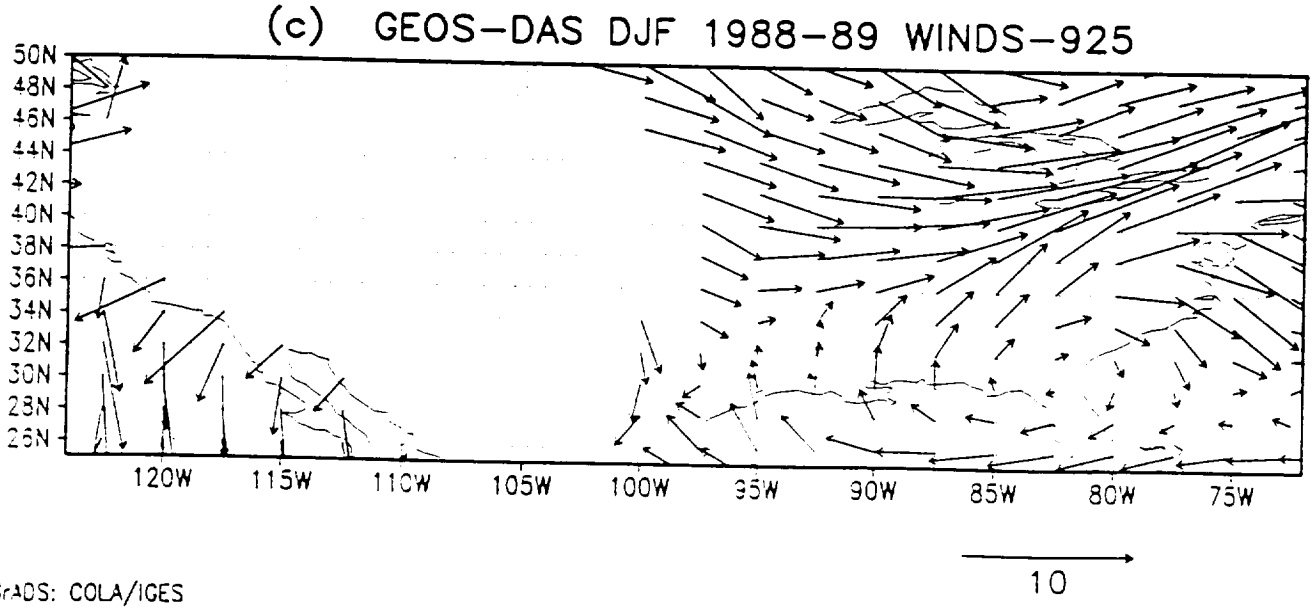

GrADS: COLA/IGES

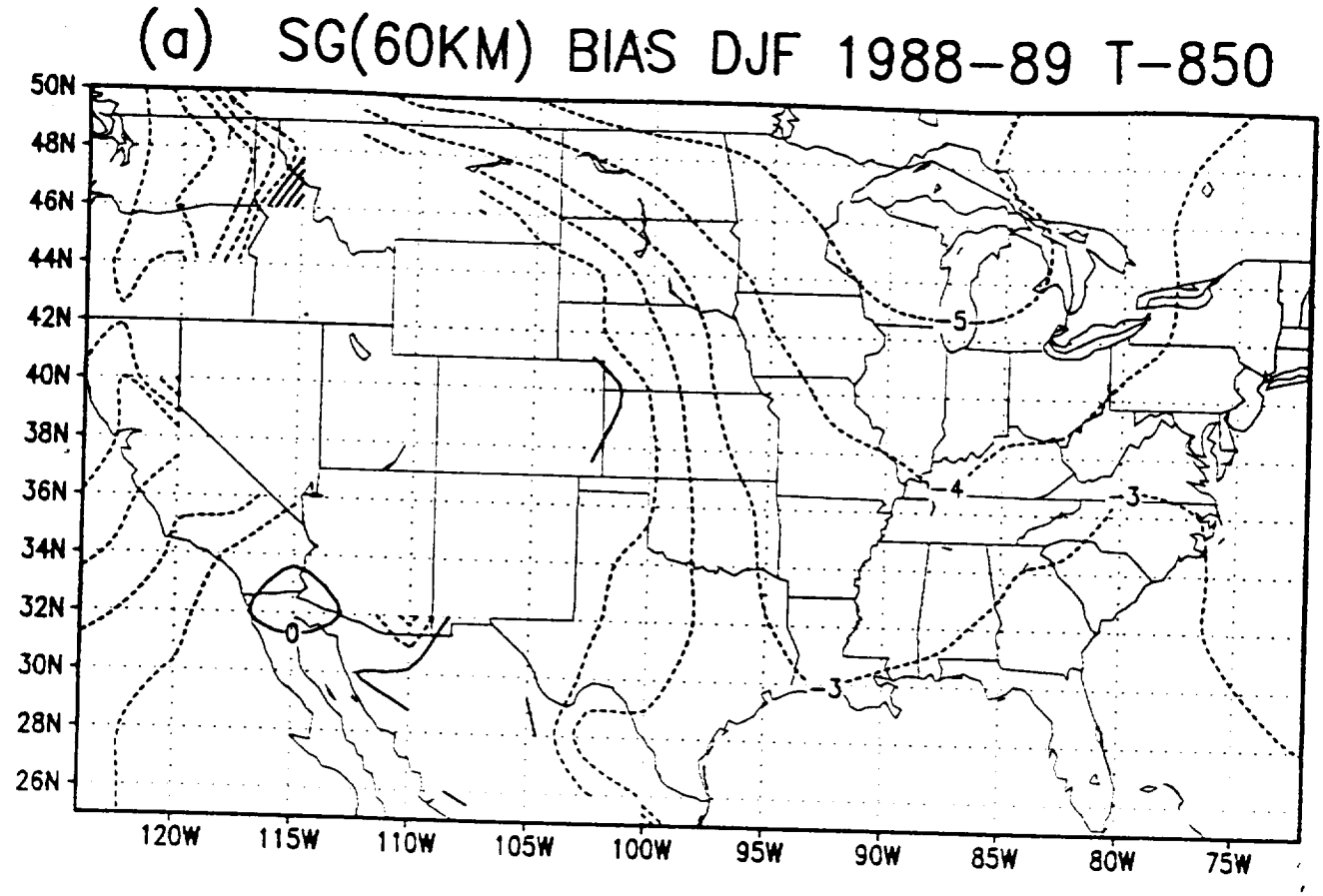
(a) SG(60KM) BIAS DJF 1988-89 T-850
50N
48N
46N
44N
42N
40N
38N
36N
34N
32N
30N
28N
26N
120W
115W
110W
105W
100W
95W
90W
85W
80W
75W
5
4
3
0
-3

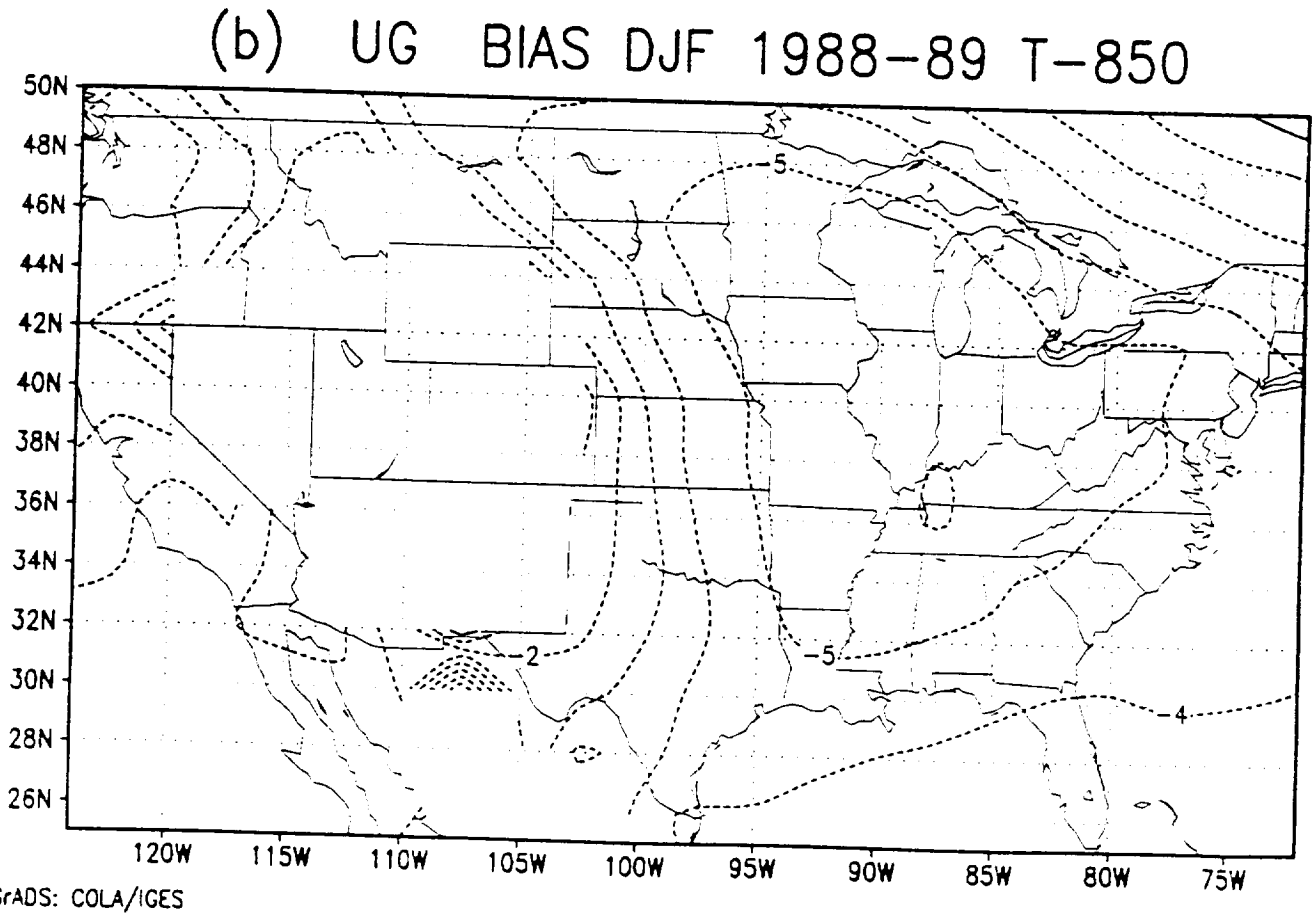
(b) UG BIAS DJF 1988-89 T-850
50N
48N
46N
44N
42N
40N
38N
36N
34N
32N
30N
28N
26N
120W
115W
110W
105W
100W
95W
90W
85W
80W
75W
5
2
-5
-4
GrADS: COLA/IGES

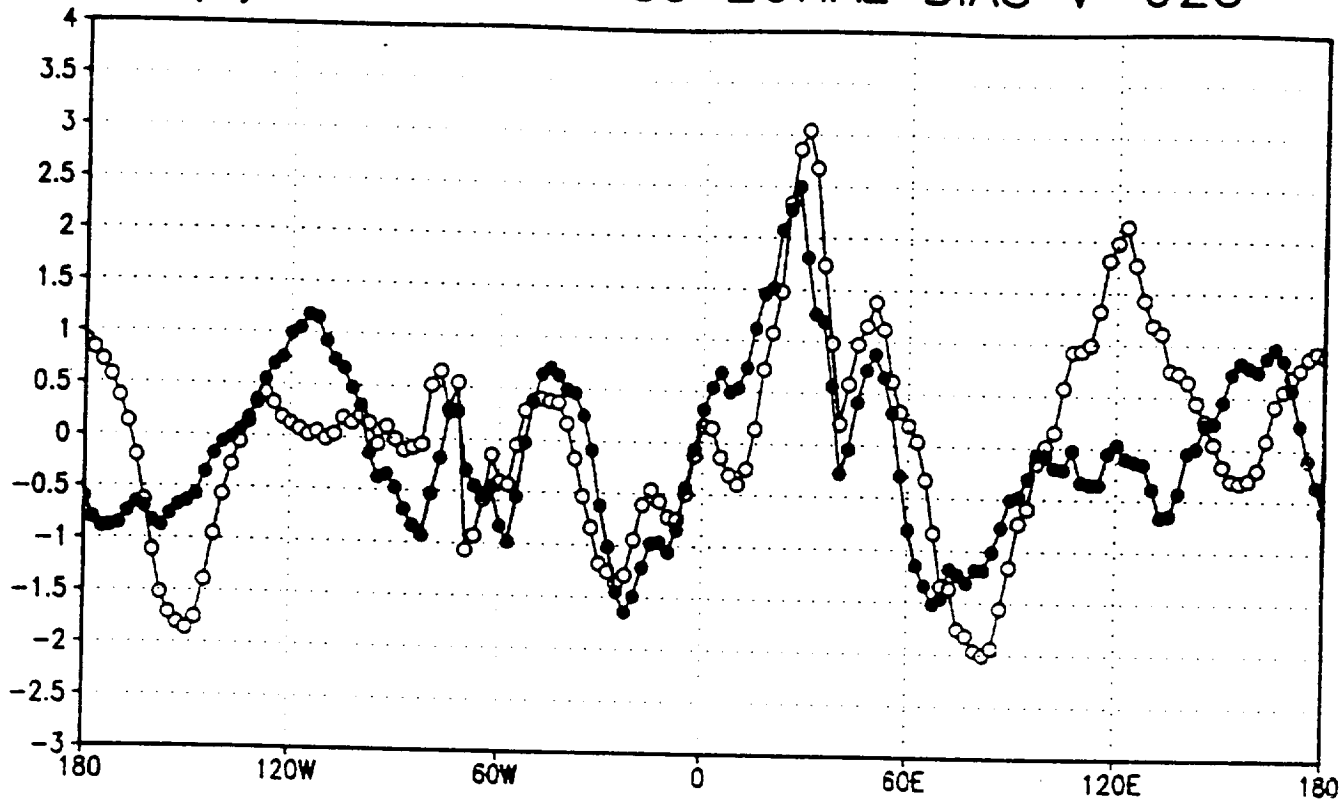

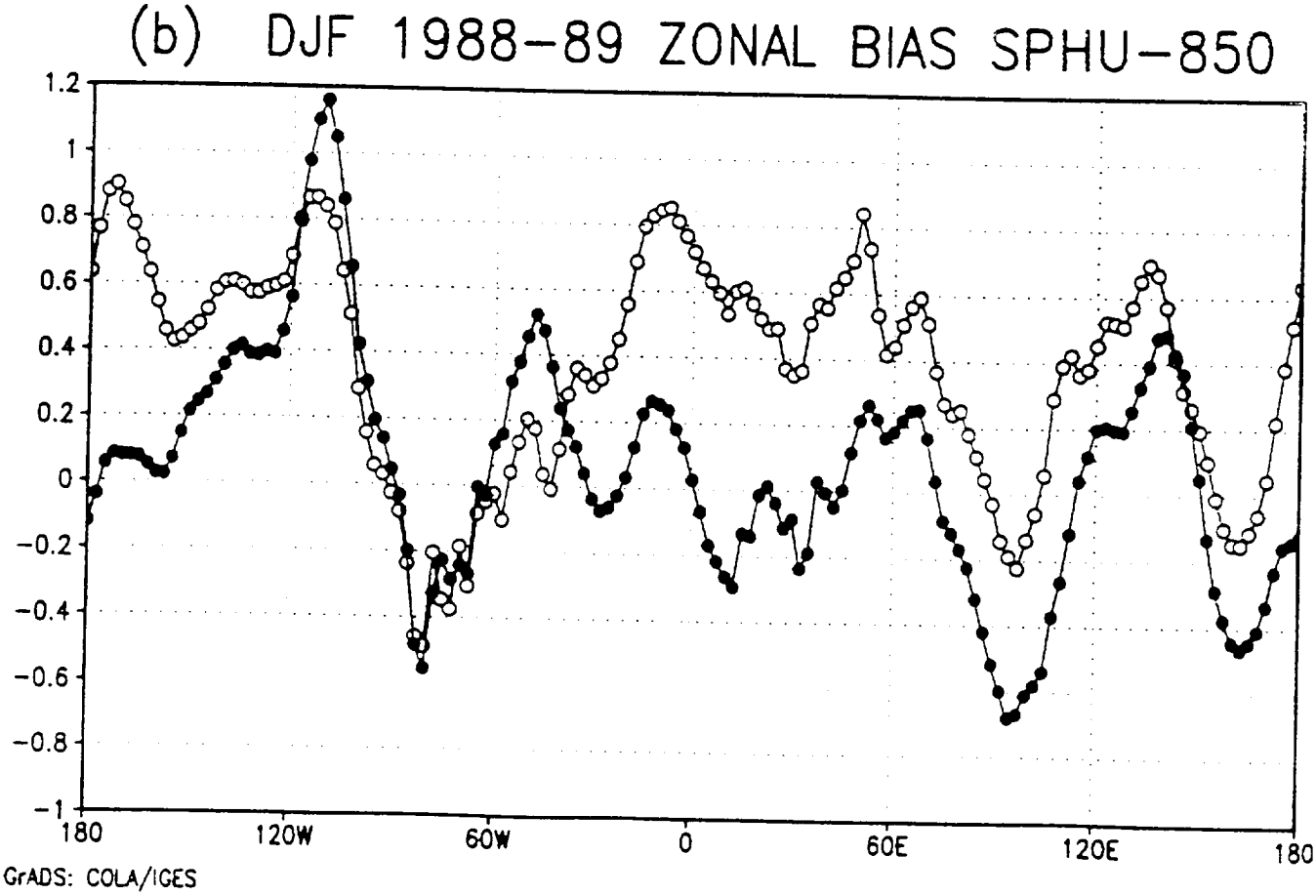

GrADS: COLA/IGES

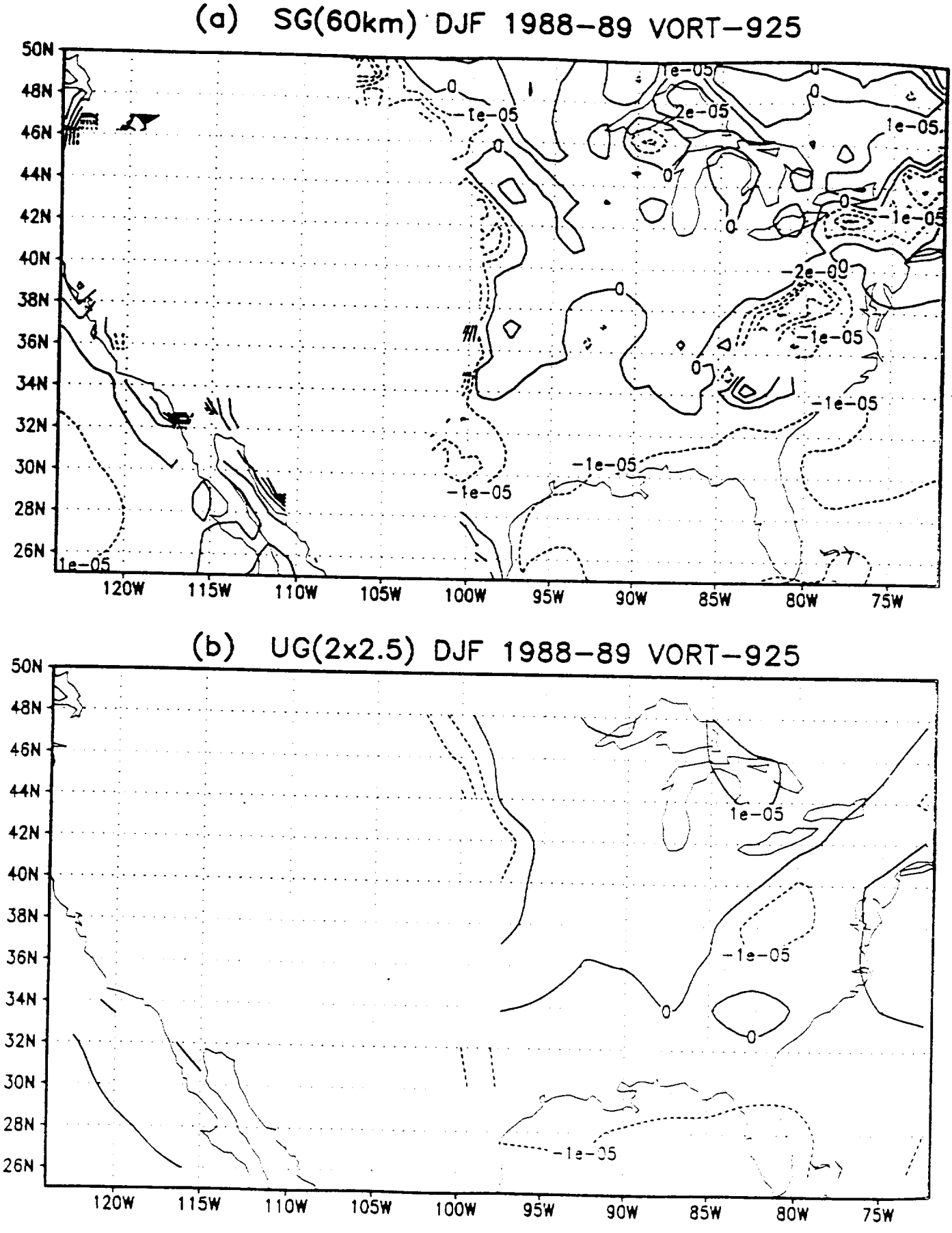

GrADS: COLA/IGES